https://doi.org/10.5194/nhess-2023-52
Preprint. Discussion started: 4 April 2023

Natural Hazards and Earth System Sciences
Discussions

Review article: Deterministic seismic hazard assessment of the area comprised between west Gulf of Cádiz and east Alboran Sea

Adrián José Rosario Beltré[1,2], Carlos Paredes Bartolomé[1], Miguel Llorente Isidro[3]

[1] Department of Geological and Mining Engineering, Higher Technical School of Mines and Energy, Universidad Politécnica de Madrid (UPM), Ríos Rosas 21, 28003 Madrid, Spain
[2] Department of Geological Resources for the Ecological Transition, Geological Survey of Spain (IGME), Spanish National Research Council (CSIC), La Calera 1, 28760 Tres Cantos (Madrid), Spain
[3] Department of Geological Risk and Climatic Change, Geological Survey of Spain (IGME), Spanish National Research Council (CSIC), Rios Rosas 23, 28003 Madrid, Spain

Correspondence to: Adrián José Rosario Beltré (aj.rosario@igme.es) Carlos Paredes Bartolomé (carlos.paredes@upm.es)

Abstract. The convergence zone of the NE-SW complex comprising the Gulf of Cádiz and the Alboran Sea, at the Eurasian-Nubian plate boundary, is frequently affected by seismic activity, caused by submarine long-strike strike-slip fault systems and arcuate fold-thrust systems found in the region. This has resulted in moderate to high magnitude earthquakes, including tsunamigenic earthquakes, and the area has also experienced tsunamis due to major earthquakes and gravitational landslides. This study carries out a Seismic Hazard Analysis, for bedrock conditions, of the marine area between the W of the Gulf of Cádiz and the E of the Alboran Sea in the Ibero-Maghrebian region, based on a deterministic approach, considering areal seismogenic sources. For the estimation of the seismic hazard, a Visual Basic script based on Excel has been used, which has been improved. The results obtained show that the most probable Peak Ground Acceleration (PGA) ranges from 0.2 to 0.4 g, although it can reach up to 1.0 g in certain areas. These results highlight the need for a detailed study of the distribution of seismic hazard in submarine areas, given the significant values of accelerations that can occur. This work is the first comprehensive deterministic seismic hazard assessment carried out in the Ibero-Maghrebian region and aims to take a first step to promote seismic hazard studies in marine areas, whose results can provide relevant information given the implications of earthquakes in the genesis of other natural hazards such as tsunamis and submarine landslides.

1. Introduction

The areas between the Gulf of Cádiz and the Alboran Sea, or the Ibero-Maghrebian region located on the Eurasian-Nubian plate boundary (Buforn et al., 1995) which comprises the southern Iberian Peninsula and the Maghreb or western part of North Africa is characterized by active tectonics with frequent seismicity, due to the continental collision tectonic contact, where the African and Eurasian plates converge. This region has been the scene of several major and devastating historical earthquakes (López Casado et al., 2000) such as the Málaga earthquake of 1680 (Mw 9; Goded et al., 2008), the

https://doi.org/10.5194/nhess-2023-52
Preprint. Discussion started: 4 April 2023


Natural Hazards and Earth System Sciences Discussions

Torrevieja earthquake of 1829 (Mw 6.8-6.9; Silva et al., 2019), the Arenas del Rey earthquake of 1884 (Mw 6.5-6.7) and those that occurred in Adra (in 1910), Motril in 1804 (Morales et al., 2003), and the Lisbon earthquake of 1755 (Mw 7. 7; Fonseca, 2020) considered this as tsunamigenic. Also, there are records of Mw 6.7 and Mw 7.3 earthquakes occurred in Asnam, North Africa, in 1954 and 1980 (Bezzeghoud et al., 2017), which triggered submarine landslides and tsunamis (Papadopoulos et al., 2014). These latter examples demonstrate the connection between earthquakes and other natural hazards such as submarine landslide and tsunamis (Collico et al., 2020).

Despite significant and recent advances in attempting to make predictions of earthquake location, time and size (e.g., Corbi et al., 2019; Tehseen et al., 2020), uncertainty remains, as the results are associated with high certainty and in most cases are not definitive. To date, the most used method is Seismic Hazard Analysis (SHA) to estimate plausible ground motions and mitigate seismic hazard and associated risks (Geller et al., 1997). Currently, the two broad standard approaches to seismic hazard analysis are Deterministic Seismic Hazard Analysis (DSHA) and Probabilistic Seismic Hazard Analysis (PSHA). Implicitly, DSHA uses "deterministic" information during the analysis (Reiter, 1990; Kramer, 1996; Campbell, 2005), in which the largest individual earthquake defined as the maximum credible, expected or characteristic earthquake (MCE) is considered, while PSHA combines probabilistic characteristics, through the distributions of location, magnitude, recurrence, of a set of earthquakes or seismic catalog, and in the attenuation ratio (Cornell, 1968), to manage and incorporate the seismic uncertainty of the earthquake space-time-size events. These methods, sometimes questioned (Bommer, 2002, 2003; Castaños and Lomnitz, 2002; Krinitzsky, 1993a, b, 2002), remain the most widely used in regional seismic hazard assessments worldwide (Orozova and Suhadolc, 1999; Mualchin, 2005; Cheng et al., 2007; Moratto et al., 2007; Pailoplee et al., 2009; Sokolov et al., 2009). Although, the approach offered by a probabilistic assessment PSHA is currently the most widely implemented by the scientific community and seismic risk assessment and mitigation plans, the DSHA is still considered useful in "worst-case" scenario modeling situations (Grasso and Maugeri, 2012; Mostafa et al., 2019). This type of scenario is standard procedure in emergency planning due to its conservative approach to risk estimation commonly used by civil protection systems. However, it should be noted that these methods DSHA and PSHA can complement each other, providing more information about the existing seismic hazard at the site under study (Wang et al., 2012).

The marine zone proposed in this work, comprised between the western end of the Gulf of Cádiz and the eastern end of the Alboran Sea, has an almost null account of seismic hazard studies, despite the importance of the region as a generating source of earthquakes, submarine landslides and tsunamis (Papadopoulos et al., 2014; Rodríguez et al., 2017; Vázquez et al., 2022). The first and only recorded attempt to assess the seismic hazard in this area was made by Molina Palacios (1998), in which the seismic hazard of the Iberia-Africa contact area was assessed based on a probabilistic approach. However, no DSHA application is available in this particular submarine region. The study area also includes some emerged areas on its borders, to the north on the southern coast of the Iberian Peninsula and to the south, on the North African coast. These, being habitable areas, do have exhaustive seismic hazard studies, using both deterministic and probabilistic approaches. In the

https://doi.org/10.5194/nhess-2023-52
Preprint. Discussion started: 4 April 2023

Iberian part, multiple probabilistic studies have been carried out (e.g., Crespo et al., 2014; Rivas Medina, 2014; Salgado Gálvez et al., 2015; IGN-UPM, 2017; Rivas-Medina et al., 2018) to date. Similarly, the seismic hazard of the city of Seville was evaluated by Sá et al. (2021) based on a deterministic approach and a Neo-deterministic Seismic Hazard Assessment (NDSHA) (Panza et al., 2001; Panza and Bela, 2020) was recently performed for the Iberian Peninsula by García-Fernández et al. (2022), being the first study of this type in the peninsula. In the North African part, the most recent PSHA was performed by Poggi et al. (2020), being one of the works used in this study as a data source. Regarding the SHA by deterministic approach, an NDSHA was performed by Mourabit et al. (2014) in this region.

The main objective of this paper is to perform a SHA, for bedrock conditions, of the marine area between the W of the Gulf of Cádiz and the E of the Alboran Sea, based on a DSHA approach, considering areal seismogenic sources. To carry out this analysis, an Excel-based Visual Basic script, which has been enhanced, was used. Also, a comparison with studies presented on the geography of the emerged terrain within the study area, carried out with other seismic hazard analysis techniques (e.g., NDSHA, PSHA), is provided to verify and validate the results obtained in the submarine zone. This work is the first comprehensive DSHA performed in the Ibero-Maghrebian region and aims to take a first step to promote the assessment of seismic hazard in submerged areas, whose results may yield relevant information for the identification of possible seismic sources that could be tsunamigenic or triggers of submarine landslides.

2. Seismotectonic setting of study area

The study region in this paper comprises the Ibero-Maghrebin-Algerian band of the Gulf of Cádiz-Alboran Sea arc, located at the present-day boundary between the Eurasian and Nubian tectonic plates (West Africa). Geographically, from west to east, the region of interest (outlined with a red polygon line in Fig. 1) extends from the Gorringe Ridge and the Horseshoe Abyssal Plain (longitude 11.5ºW) in the west up to the Algerian compression belt (longitude 2ºE) in the east (Fig. 1), with the Gibraltar Arc, the deformation front of the Betico-Rif orogenic belt and related structures in the centre (Vázquez and Vegas Martínez, 1999). The northern edge is bounded from WNW to ESE at latitude 38ºN, by the Algarve region to the Guadalquivir basin, where it runs parallel to the ENE-WSW Cenozoic reverse fault line, along the southern boundary of the Guadalquivir depression with the Baetic and its extension to Cabo de la Nao, the beginning of the Valencia trough. To the south, it follows the trace of the Gibraltar fault WNW-ESE at latitude 34ºN to the Rift and from there it takes an ENE-WSW direction parallel to the Algerian Mediterranean coast along the southern boundary of the Atlas Mountains to the Algerian compression belt (Buforn et al., 1995).

The structures that tectonically compose this region are still active today. As shown by geodetic data and geodynamic studies that have been carried out for decades (e.g., Montessus de Ballore, 1894; Pastor, 1927; Munuera, 1963; Buforn et al., 1995; Negredo et al., 2002; Soumaya et al., 2018), tectonic models of NW-SE to WNW-ESE oblique convergence between the plates (Reilly et al., 1992; Herraiz et al., 2000) present displacements of 2 to 5 mm/yr (Nocquet, 2012) of the western

https://doi.org/10.5194/nhess-2023-52
Preprint. Discussion started: 4 April 2023

Natural Hazards and Earth System Sciences
Discussions

Baetic Cordilleras with respect to the Iberian Massif (Koulali et al., 2011; Palano et al., 2013; Gonzalez-Castillo et al., 2015). The complex geodynamic context of interaction between the Eurasian and Nubian plates characterises the tectonics affecting the seafloor of the Gulf of Cádiz (Medialdea et al., 2004; Custódio et al., 2016; Neres et al., 2016) and Alborán Sea regions (Stich et al., 2006; Martínez-García et al., 2011; Estrada et al., 2018; Lafosse et al., 2020; Galindo-Zaldivar et al., 2022; Gómez de la Peña et al., 2022), makes it the most geologically active area in the western Mediterranean, affected by marine and also terrestrial geological hazards, given its moderate to low-moderate seismic activity, as attested by historical cases (Vázquez et al., 2022a).

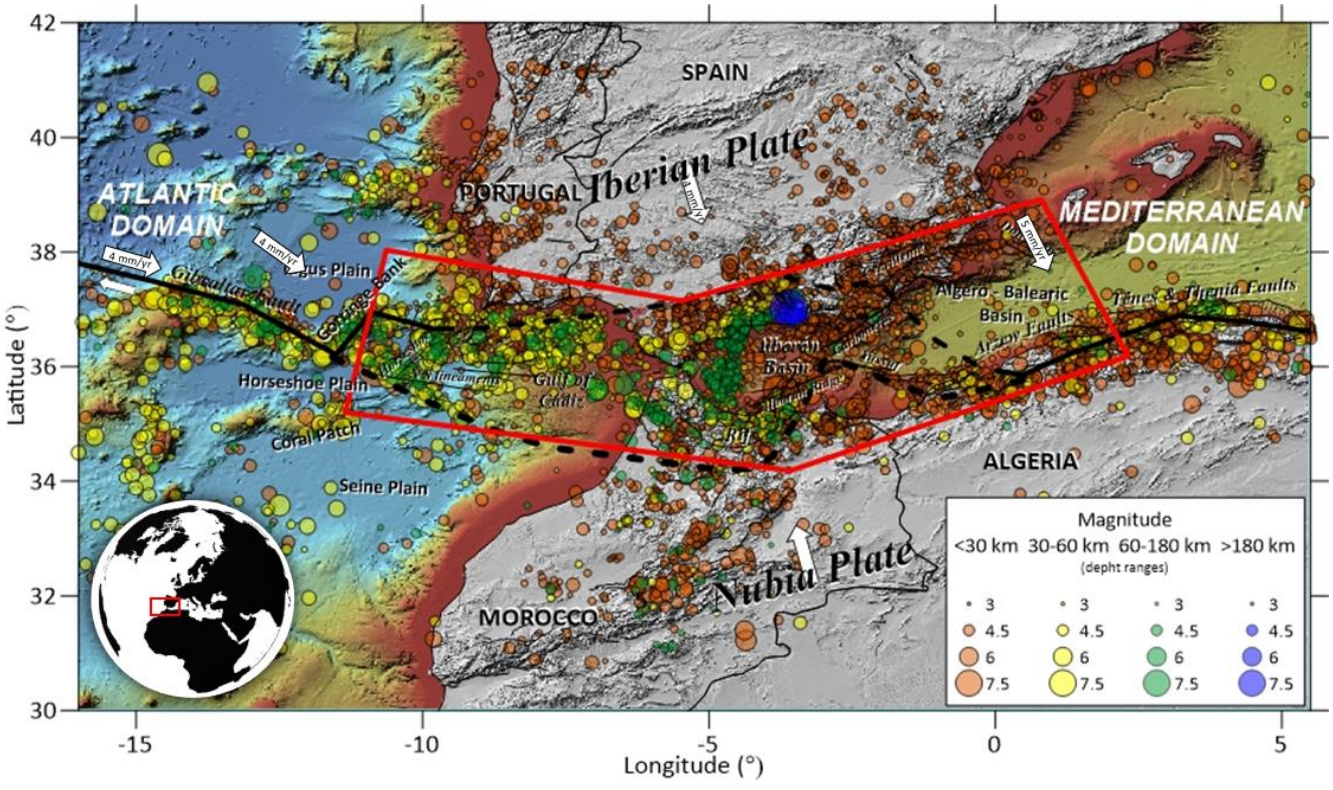

Figure 1. Red polygon shows the study Ibero-Magrebi-Algerian area in this work comprising west Gulf of Cádiz to east Alboran Basin. Simplified seismotectonic map of study area between Nubia and Iberian Plates (infered modern boundary: thick black line, white arrows: relative movement direction between plates). Earthquake epicenters located according to their magnitudes and depth (circle size and colour in legend) distribution from IGN catallogue (available from https://www.ign.es/web/ign/portal/sis-catalogo-terremotos). Background: shadowed Digital Terrain Model (altimetry and bathymetry) in the study area (extracted from GEBCO, 2020).

The Gulf of Cádiz is located on the contact boundary between the Eurasian and African plates, which runs, in its westernmost part, from the Azores Islands to the Strait of Gibraltar, through the Iberian massif and the Algarve basin to the north, and, in the eastern part, through the orogenic arc of the Betic-Rifenean mountain range, the westernmost of the

https://doi.org/10.5194/nhess-2023-52
Preprint. Discussion started: 4 April 2023


Natural Hazards and Earth System Sciences Discussions

Mediterranean alpine chains. It is characterised by a NW-SE oblique convergence regime, mainly controlled by the formation of the Betic-Rifene orogen and by the accommodation of post-orogenic compressional tectonic activity (IGN, 2023). This means that seismic activity in the Gulf of Cádiz is important, with mainly shallow earthquakes (h < 30 km), without clearly marking a subduction zone, and of moderate magnitude (Martín-Dávila and Pazos, 2003). Most of the focal mechanisms in this area are reverse and rifting type with a maximum horizontal compression in a NW-SE direction. However, there is historical and instrumental evidence of high-magnitude earthquakes in the region. These include the earthquakes of 1755, with an approximate magnitude of 8.5, and of 1969, with a magnitude of 7.8, which caused a small tsunami on the coasts of Morocco, Portugal, and Spain. Geological structures such as the Gorringe Bank, San Vicente submarine canyon, and the Nazaré and Cádiz-Alicante faults coincide with the areas of greatest seismicity in the region.

The Alboran Sea is the westernmost part of the Mediterranean Sea, bordered both to the north and to the south by the Alpine mountain ranges of the Betic, to the south of the Iberian Peninsula, and the Rif in the north of the African continent. It is a complex contact zone between the Eurasian and Nubian tectonic plates, its genesis and evolution are related to the process of convergence between these plates, due to the northward push of the African plate. This compressional tectonic process generated a constant westward migration of the Alboran domain (tectonic microplate that includes the internal zones of the Betic and the Rif), leading to the formation of the aforementioned alpine mountain ranges and a distensional basin with lithospheric thinning of the continental crust, with associated volcanism, which gave rise to the island of Alboran. Among the tectonic structures, the submarine mountain ranges stand out, with a length of more than 50 km, with a NE-SW orientation, and delimited to the north and south by reverse faults with opposite dip. On the other hand, there are two sets of conjugate directional faults: NNE-SSW sinistral faults such as the Al-Idrisi fault, or NE-SW faults such as the Carboneras fault, and NW-ESE dextral faults such as the Yusuf fault. The maximum magnitudes recorded in the Alboran Sea have lower values. The most important events are the Adra earthquakes in 1910 with Mw 6.1 (Stich et al., 2003), 1994 with Mw 6.4 (e.g., El Alami et al., 1998), 2004 with Mw 6.3 (Galindo-Zaldívar et al., 2009) and 2016 with Mw 6.3 (Galindo-Zaldivar et al., 2018).

The Maghreb-Algerian region as far as Tunisia is a key area in the western Mediterranean to understand the active tectonics and stress pattern across the slowly converging oblique Africa-Eurasia plate boundary. Its seismic activity is interconnected with seismic activity in the Iberian Peninsula (Mantovani et al., 1989), given its location in the complex tectonic system resulting from the interaction between both plate boundaries and alternating systems of rift and reverse faults (e.g., Mourabit et al., 2014; Leprêtre et al., 2018) running E-W from the Rif in the Western Alboran Basin, eastern margin of the Strait of Gibraltar, to Tunisia along the Sardania Channel, on the Alpine Tell/African Maghrebides chain (Buforn et al., 2004; Meghraoui and Pondrelli, 2012). Its seismotectonic configuration, which forms an extensive belt of northwest African folds and thrusts and fault systems, where a complex compressional regime prevails, is what gives this region its seismicity. In particular, the current active contraction of the West Africa-Eurasia boundary is accommodated by a strike-slip fault

https://doi.org/10.5194/nhess-2023-52
Preprint. Discussion started: 4 April 2023


Natural Hazards and Earth System Sciences Discussions

regime with a normal component in the Alboran/Rif block, a predominantly NE-SW thrust fault with a strike-slip component in the western part of the Tell, and an E-W strike-slip fault with a reverse component along the eastern Tell and the Saharan-Tunisian Atlas (Soumaya et al., 2018), Subordinate NE-SW left-lateral strike-slip faults are also present. The seismic events and corresponding stress distribution generated by these fault systems are distributed with a general E-W trend and a NW-SE shortening component along the Africa-Eurasia plate boundary (Ousadou et al., 2014).

Large earthquakes occur in the areas of the Gulf of Cádiz-SW of Cape St. Vincent and NW of Algeria. Smaller earthquakes occur in the S and SE Iberia and N Morocco. The vast majority (Fig. 1) have shallow foci (h < 50 km), although a significant number of earthquakes are also generated at intermediate depth (50-200 km) and some very deep earthquakes (600-670 km). Deep earthquakes are located in the province of Granada (south of Dúrcal-Alborán Sea) (Molina Palacios, 1998; Buforn and Udías, 2007). Intermediate seismicity is mainly located in the areas of the Gulf of Cádiz, mainly located within the crust up to a depth of 100 km; about 90% of the observed seismicity occurs at approximate depths up to 55-60 km in the Gorringe Bank, High Atlas and in the Granada-Málaga-O de Alboran area. In the Alboran Sea there is also significant shallow seismicity at depths of less than 30 km, especially in the active Betica-Alboran-Rif shear zone; from here onwards to the W it becomes much deeper. Due to the fact that most of the seismicity is shallow, it is expected that in the future moderate to high-magnitude earthquakes could occur, generating important deformations in the seabed that could be the origin of tsunamis, such as those that have been generated in historical and recent times in the area near the Maghreb-Algerian coast (Mourabit et al., 2014), or that may destabilise the seabed, giving rise to submarine landslides (Maramai et al., 2014; Somoza et al., 2021).

3. Materials

3.1 Ocean and land digital terrain models

The mid-resolution digital terrain model (DTM) used in this study was constructed from a gridded data set developed by the four Regional Centres of the Nippon Foundation-GEBCO Seabed 2030 Project (Mayer et al., 2018; GEBCO Compilation Group 2022, 2022). This global terrain model for ocean and land with a spatial resolution of 15 arc seconds is produced from version 2.4 of the SRTM15+ base grid (Tozer et al., 2019) augmented with measured and estimated seafloor topography from shipboard beam echosounders and depths predicted using satellite altimetry, from the European Marine Observation and Data Network (EMODnet; http://www.emodnet.eu/). This global continuous terrain gridded model provides elevation data (altimetry > 0 and bathymetry < 0) in metres. The GEBCO_2022 Grid compilation was carried out at the Seabed 2030 Global Centre, hosted at the National Oceanography Centre, UK.

The original DTM GEBCO grid for this paper has been downloaded over a rectangle area 12ºW 34ºN to 3ºE 39ºN (background in Fig. 1), from the Internet in netCDF (CF Compliant), Esri ASCII raster, or GeoTiff data formats. To adjust

https://doi.org/10.5194/nhess-2023-52
Preprint. Discussion started: 4 April 2023

the comparison of the results obtained in this work with those obtained in the seismic hazard analysis in areas comprising the study area, the original spatial resolution of 15 arc-seconds (about 450 m x 450 m) raster file, which data values are pixel-centre registered, has been resampled by averaging to 0.1º x 0.1º grid resolution, corresponding to cells with approximately 10 km in latitude.

3.2 Seismogenic Source Catalogues and Seismicity Parameters

Currently, the Ibero-Maghrebian region does not have its own seismogenic source zonation model that covers it in its entirety or, at least, the regions of the Gulf of Cádiz, the Alboran Sea, and North Africa as a whole, which are included in the study area of this work. However, several models already proposed and accepted by the scientific community, which, if correctly integrated, could be used to compose such a zonation. These three regions, although governed by the same regional tectonic framework resulting from the oblique interaction of the Eurasiatic and Nubian-African plates, have very heterogeneous seismic and seismotectonic characteristics, resulting in a diversity of seismogenic zones when forming models to characterise the distribution of seismicity in these regions.

There are several seismogenic zonation models that partially cover the study area (Fig. 2). The ZESIS or COMMISSION zonation model (García Mayordomo, 2015), used to update the seismic hazard map in Spain (IGN-UPM, 2017), whose southern boundary runs along the NW-SE Gibraltar-Azores fault to the Moroccan Rif where it takes a WSW-ENE direction, running parallel to the Algerian Mediterranean coast. Models considered for the development of the Portuguese seismic hazard map include the ERSTA (Carvalho and Malfeito, 2018) and the EC8 (CEN, 2004) whose southern edge runs similarly to the Spanish model. The zonation of the Harmonisation of Seismic Hazards in Europe Project, or SHARE project (Giardini et al., 2014; Woessner et al., 2015), designed for the 2013 Euro-Mediterranean Seismic Hazard Model (ESHM13) at the European scale for the Euro-Mediterranean region. All of these partially cover the regions of the Gulf of Cádiz and the Alboran Sea, and very slightly cover the seismogenic activity of North Africa. Therefore, the zonation for the North African region proposed by Poggi et al. (2020) has also been considered. All these models use seismogenic sources of an areal type, with the incorporation of certain active faults as independent and complementary seismogenic sources to the characterisation of the areal zones.

In this study we opted to integrate different models into an areal seismogenic zonation model covering our studied region, analysing their compatibility. Among the previous seismic zonation models, the selected models, together with their corresponding characteristic seismic parameters, were the ZESIS (Fig. 2a) and the NAF model proposed by Poggi et al. (2020) (Fig. 2b), as they are the most recent models and are in the best geographical conditions as they overlap widely in the study area of this work, considering initially of interest the areal seismogenic sources that are within the limit (perimeter marked in red in Fig. 2) in both models, in this way, in addition to making an integration of both models, the NAF in the north can be complemented with the ZESIS, and the ZESIS east in the south with the NAF.

https://doi.org/10.5194/nhess-2023-52
Preprint. Discussion started: 4 April 2023

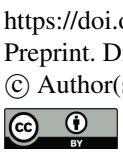

Natural Hazards and Earth System Sciences
Discussions
Open Access
EGU

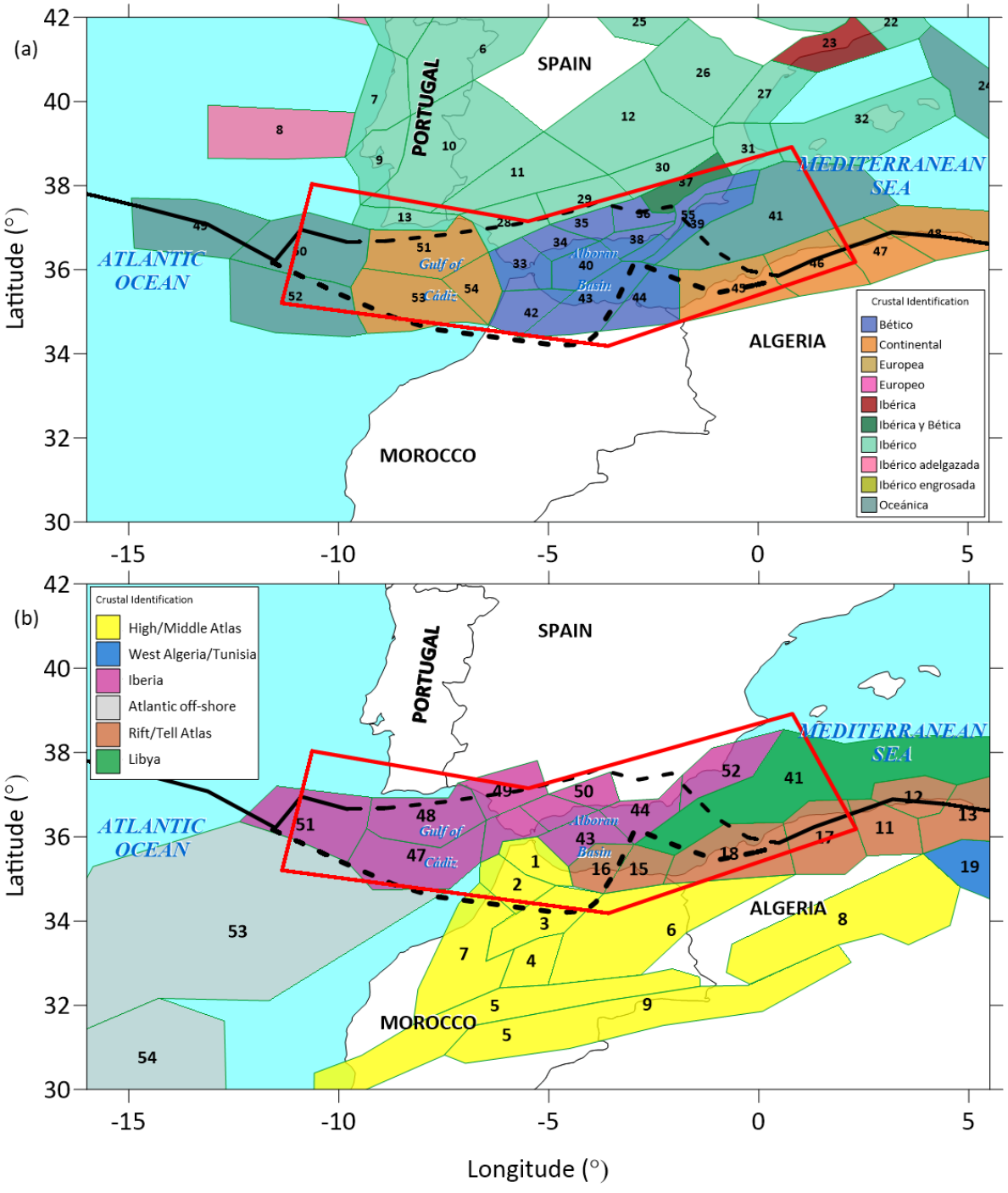

Figure 2. Seismogenic zones in the stable continental crust in the region (SACR). Colours are used to represent the tectonic groups of the SACR: (a) model for South Iberia (modified from ZESIS: IGN-UPM, 2017) and (b) model for North Africa (modified from NAF: Poggi et al., 2020).

https://doi.org/10.5194/nhess-2023-52
Preprint. Discussion started: 4 April 2023


Natural Hazards and Earth System Sciences Discussions

4. Seismic hazard assessment

Seismic hazard is the probability that an earthquake occurs in a given geographic area, within a given time period, and with a ground motion intensity exceeding a given threshold (McGuire, 2004). It is generally quantified as the frequency with which the amplitude of ground motion caused by seismic events at a given point on the ground surface is exceeded during a specified period of time. Seismic Hazard Analysis (SHA) performs the assessment of the expected ground motion caused by a seismic event for a given location (Kijko, 2019) by describing the potential for an earthquake-related natural hazard phenomenon to occur, such as strong vibrations, soil liquefaction processes, etc. Seismic hazard can be expressed in different ways, but most often in terms of values or probability distributions of accelerations, velocities, or displacements of bedrock or ground surface. Several methods are used to assess seismic hazard. The most commonly used are DSHA, PSHA, and current variants of DSHA such as the NDSHA (Panza et al., 1996, 2001, 2012; Magrin et al., 2017; Panza and Bela, 2020). Although both methods use seismological and geological information, they define and calculate seismic hazard differently, which improves the understanding of seismic hazard forecasting at the studied site or region (US NRC, 1997; Benito and Jiménez, 1999; Orozova and Suhadolc, 1999; Wang and Cobb, 2012). This complementarity is one of the main reasons why in this work, in the absence of a probabilistic seismic hazard map of the entire proposed area, it has been chosen to start the preliminary study with the DSHA.

In DSHA, seismic hazard is defined as the median (50% percentile) or other selected percentile (e.g. 84% or 98% used in this work) of ground motion from a single earthquake or set of earthquakes, and is calculated from simple earthquake and ground motion statistics (Krinitzsky, 1995, 2002) that assumes a particular earthquake scenario. In PSHA, seismic hazard is defined as ground motion with an annual frequency or exceedance rate, and is calculated from a mathematical model based on statistical earthquake and ground motion relationships (McGuire, 2004, 2008), in which uncertainties of earthquake size, moment, and size are explicitly considered (Kramer, 1996). PSHA methods are further classified into parametric (Cornell, 1968; Kramer, 1996) and nonparametric (Gumbel, 1958; Epstein and Lomnitz, 1966) methods, which differ in that the former rely on the total probability theorem and the latter use extreme value distribution functions when assessing seismic hazard.

In any of the above methods, a key component of any seismic hazard assessment is the ground motion attenuation ratio, called the ground motion prediction equation (GMPE). The DSHA determines the ground motion of a single earthquake or of several earthquakes with a maximum impact. It calculates the ground motion of individual earthquakes (i.e., maximum magnitude, maximum likelihood, or maximum likelihood) from the result, with an allowable uncertainty excess rate, provided by the GMPE. And for the PSHA, as demonstrated by (Cornell, 1968; Cornell et al., 1971), the exceedance probability for a given ground motion can be obtained from a likelihood analysis of the GMPE.

https://doi.org/10.5194/nhess-2023-52
Preprint. Discussion started: 4 April 2023


Natural Hazards and Earth System Sciences Discussions

4.1 Ground motion prediction equations (GMPEs)

One of the most important parts of evaluating seismic hazards is determining the ground motion model, which is a mathematical formula that predicts how an earthquake will affect the ground. This formula is known as the ground motion prediction equation (GMPE). These attenuation functions are commonly derived from strong ground-motion records for an earthquake of magnitude M occurring at a distance R or seismic scenario (M,R), where M is the moment magnitude, and R is the distance metric related to the energy path between the source and the site, over a range of magnitudes and distances that are meaningful for the analysis. With an appropriate set of quality records, it is possible to fit a parametric model f(M,R,{pi}) to estimate the intensity of strong motion Y for a given seismic scenario. Due to the dispersion of the recorded data pairs (M,R), resulting from the randomness introduced by the natural environment, the correlation between variables can be strong, but never perfect, so there is an unavoidable error in these regression models. If the expected seismic intensity at the project site Y is interpreted as a conditional random variable on the pair (M,R), the models $Y \sim f(M,R,\{p_i\})$ provide an estimate of the median and the error term οφ τηε ιντενσιτψ of the ground motion in terms of magnitude of the earthquake, distance and site, and rupture and geological conditions. Due to the frequent lognormal behaviour of the recorded Y values at different locations and conditions, it depends on the energy released by the earthquake and how this is dissipated in the path from its hypocentre to a site located at a certain distance, which is usually formulated as:

$$L(Y) = f(M,R,\{p_i\}) + \varepsilon = f_1(M^{\alpha}) + f_2(R^{-\beta}) + f_3(e^{M}) + f_4(R) + f_5(\{p_i\}) + \varepsilon \quad (1)$$

This formula, in which L(Y) is the natural or in base 10 logarithm of the seismic intensity Y, provides an estimate of the maximum ground motion at a point, after attenuation with the distance that the original shaking level in a forthcoming earthquake, based on its magnitude M, the distance from the source to the evaluation point R, the lithological characteristics of the geological medium traversed, and the rupture mechanism involved in the earthquake, mainly.

This expression (1) of the GMPE is composed of the sum of different terms $\{f_i(\cdot)\}$ that quantify the attenuation of the energy transported by the seismic wave train through the geological medium. In general, these terms are: f_1, a term proportional to M^{α}, since the magnitude is defined as the logarithm of some maximum motion parameter; f_2 a term proportional to $R^{-\beta}$ since the propagation away from the earthquake source through the geological medium of the energy waves causes the amplitudes of the body waves to decrease as a function of R^{-1}, and the amplitudes of the surface waves to decrease as a function of $1/R^{-0.5}$; f_3 is a term that incorporates that the area in which fault rupture occurs increases with increasing earthquake magnitude, so that some of the waves that produce strong motion at a location arrive from a distance, R, and others arrive from greater distances, so the effective distance is therefore greater than R by an amount that increases as the magnitude increases; f_4 includes the damping of the energy carried by the deformation waves by the geological material traversed which causes the ground motion amplitudes to decrease exponentially with R; and, lastly, f_5 introduces through a series of parameters $\{p_i\}$ the possible effect of source characteristics or geological ground conditions on the

https://doi.org/10.5194/nhess-2023-52
Preprint. Discussion started: 4 April 2023


Natural Hazards and Earth System Sciences Discussions

ground motion. Finally, the error term ε is identified by a Gaussian distributed random variable, with null mean E[ε] =0 and variance Var[ε] = σ^2 or random dispersion around the behaviour of the model expressed in (1), resulting from the recorded seismic data used in its empirical regression. Catalogues of GMPEs for different regions of the world and various Y-motion parameters contain some relationships that use all these terms, their combinations in varying degrees of complexity, and others that do not (Douglas, 2001, 2020).

Most GMPEs (1) are defined in terms of finite metrics of fault distance assuming a planar rupture geometry. The rupture trace is defined as the projection of the upper edge of the rupture onto the ground surface. The rupture plane, trace, and surface projection allow the definition of four finite fault distance metrics used in GMPEs: R_{RUP}, R_{JB}, R_X, R_Y, Z_{TOR} (Fig. 3). The rupture distance R_{RUP} is the distance from the site to the nearest point of the rupture plane. The Joyner-Boore distance R_{JB}, is the closest distance between the site and the surface projection of the rupture plane, and the auxiliary parameters R_X, R_Y, and Z_{TOR} are the coordinates from the site to the closest point of the top of the rupture (Kaklamanos et al., 2011). Depending on which distance metric the GMPE is formulated, there may be cases where the estimation of the intensity of the movement is affected by the relief of the terrain where the site is located. Therefore, if the terms of expression (1) involving R are given as a function of R_{RUP}, R_Y, or Z_{TOR}, the effect will be more noticeable if Y is evaluated in mountainous areas, providing lower values as the distance increases, or at marine depths, obtaining higher Y because they are closer to seismogenic sources, so it is expected that the results of the estimation of Y in regions with significant unevenness will be sensitive to the use or lack of a DTM of the area.

Unfortunately, the scarce availability of strong motion records for the whole Ibero-Maghrebian marine area, due to the lack of sufficient records in the southern Iberian Peninsula and North Africa, merits a selection of a set of more representative GMPEs, without the possibility of direct comparison (Atkinson et al., 2014) with local earthquake records, in a meaningful range for the (M,R) scenarios. Therefore, instead, nondirect selection criteria have to be used, paying special attention to the adequacy of the tectonic context and the suitability of the GMPE functional form (Cotton et al., 2006; Poggi et al., 2020), relying on SHA work that has been carried out in the emerged zones, southern Iberian Peninsula and North Africa, bordering the study area.

Recent tectonic classifications (Chen et al., 2018; Poggi et al., 2020; Hasterok et al., 2022) distinguish much of the study region as a zone of active Variscan-Hercynian surface crust (ASCR), surrounded by stable continental cratons in the central African area to the south and the central Iberian Peninsula to the north, and by a stable Atlantic oceanic region to the west. The fact that the Ibero-Maghrebian off-shore area is geographically located at the confluence of oceanic crust, active continental crust, and stable continental crust complicates the selection of suitable ground motion models. The GMPEs for active tectonic regions strongly underestimate the response spectrum ordinates for western Iberia. However, the analysis does not support that the ground motion attenuation for offshore earthquakes is anomalously low, because GMPEs developed for stable continental regions can in general reproduce them by applying a higher weighting (Vilanova and

https://doi.org/10.5194/nhess-2023-52
Preprint. Discussion started: 4 April 2023

Natural Hazards and Earth System Sciences
Discussions

Fonseca, 2012). Therefore, the set of GMPEs chosen for the area can be applied uniformly over the whole area without distinction, as it is assumed that in the ASCR there is a homogeneous behaviour of the crust in the ground motion response to seismic shaking. According to this classification, two equally weighted models (Chiou and Youngs, 2008 and Akkar and Bommer, 2010) are applied (Poggi et al., 2020) for the stable continental crust and the ASCR of the North African zone. In addition, from the latest update of seismic hazard maps in the Iberian Peninsula developed in Portugal (Vilanova and Fonseca, 2007; Silva et al., 2015) and Spain (IGN-UPM, 2017), the discrimination of GMPEs applied for the continental coastal zone has been made according to their range of validity on the seismic scenarios that may occur in the study area for magnitudes greater than 5 by selecting three GMPEs (Boore and Atkinson, 2008; Cauzzi and Faccioli, 2008; Bindi et al., 2011) that complement the two provided by the North African model. For deep seismogenic zones, two attenuation functions (Youngs et al., 1997 and Zhao et al., 2006) incorporated in the Spanish hazard update model (IGN-UPM, 2017) have been taken.

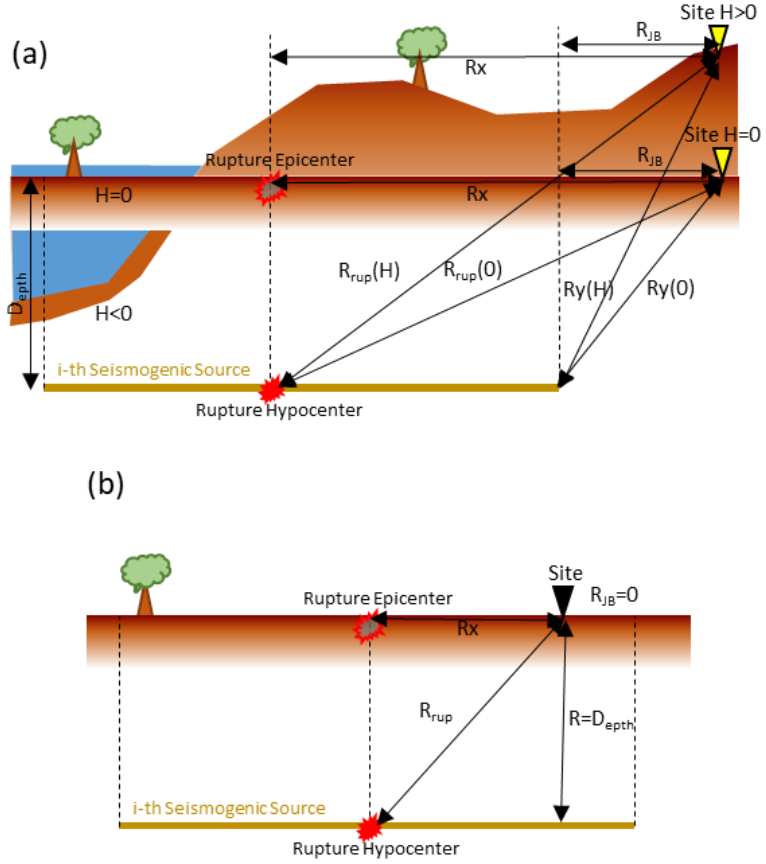

Figure 3. Earthquake source and distance measures from a evaluation site in a vertical cross-section trought a seismogenic source area: R_{JB}: Joyner-Boore distance, R_{rup}: rupture distance Rx: horizontal ground surface projection of rupture distance. (a) Site outside the ground projection of the seismogenic source, with (H≠0) and without surface altimetry or bathimetry (H=0). (b) Site inside the ground projection of the seismogenic source, without surface altimetry or bathimetry (H=0).

https://doi.org/10.5194/nhess-2023-52
Preprint. Discussion started: 4 April 2023


Natural Hazards and Earth System Sciences Discussions

At the European scale, in the ESHM13 of the SHARE project, GMPEs and their weights have been established so that the logic tree captures the epistemic uncertainty in ground motion prediction for six different tectonic regimes in Europe (Delavaud et al., 2012). For active shallow crustal regions with compression-dominated zones (a), including thrust or reverse faults, associated transcurrent faults (e.g., rift faults), Delavaud et al. (2012) recommend three GMPEs (Cotton et al., 2006; Cauzzi and Faccioli, 2008; Bindi et al., 2011) if a European database is used, or three alternative (Boore and Atkinson, 2008; Chiou and Youngs, 2008; Akkar and Bommer, 2010) if a European database is not used, which are first in their ranking based on log-likelihood and have an appreciably higher data support index (DSI) than the rest. From the preselection of these six models, the authors extract the models selected by experts for the ASCR, which are the majority of those considered in this paper. Lastly, the European-scale probabilistic SHA model has also been implemented in the Global Earthquake Map OpenQuake Engine (GEM-OQ; Pagani et al., 2014, 2020) engine, with the selection of the four SHARE strong motion models (Zhao et al., 2006; Cauzzi and Faccioli, 2008; Chiou and Youngs, 2008; Akkar and Bommer, 2010) for the ASCR (Woessner et al., 2015).

Hence, the seven GMPEs have been selected for their compatibility (Fig. 4a for the GMPEs in the ASCR) with the set of seismotectonic characteristics of the study region, considering the updating works of the seismic hazard maps in Portugal, Spain, and North Africa and the European revisions of the SHARE and GEM-OQ projects. Although the degree of relative importance or weighting of each GMPE has been adjusted, considering that they apply equally over the entire extent of the ASCR, according to the values observed at points (control cities) in emerged territory. For AKBO10 in particular, the coefficients of Bommer et al. (2012) have been incorporated, and the distance applied in CAFA08 is limited to 15 km below, in accordance with the recommendations made by GEM-OQ in its inventory of GMPEs. The magnitude of the seismic intensity Y used in all selected GMPE models is the PGA.

The types of strong motion considered include the full range of MCE for the zonings used in this work, since the minimum MCE is 5.7, higher than the maximum level (M = 5) of application of the model for low magnitudes, according to the range of magnitudes for Spain and North Africa. The BOAT08 model (Boore and Atkinson, 2008) has an uncertainty in Ln(Y) of $\sigma = 0.564$, with Y in g, is valid for the entire magnitude range, uses the Joyner-Boore R_{JB} distance in its formulation, recommended when the fault geometry is unknown, for focal depths between 2 km and 31 km, and a formulation parameterised according to the focal rupture mechanism (reverse, normal, or rupture-tear). The AKBO10 model (Akkar and Bommer, 2010) has been used in its updated rock version (Bommer et al., 2012), as recommended by GEM-OQ (Giardini et al., 2013; Woessner et al., 2015), to obtain log(Y), with the PGA in cm/s^2, considering a formulation in three categories according to the failure mechanism, using the R_{JB} distance and uncertainties $\sigma_1 = 0.2610$ (intra-event) and $\sigma_2 = 0.0994$ (inter-event). The CAFA08 model (Cauzzi and Faccioli, 2008) provides log(Y) where Y is in m/s^2, with an uncertainty of $\sigma = 0.344$ for the horizontal PGA, taking a reference shear wave velocity in the upper 30 m (V_{s30}) of 800 m/s, corresponding to soil type A, according to Eurocode-8 and the RJB distance modified with the depth to the source. The

https://doi.org/10.5194/nhess-2023-52
Preprint. Discussion started: 4 April 2023

Natural Hazards and Earth System Sciences
Discussions

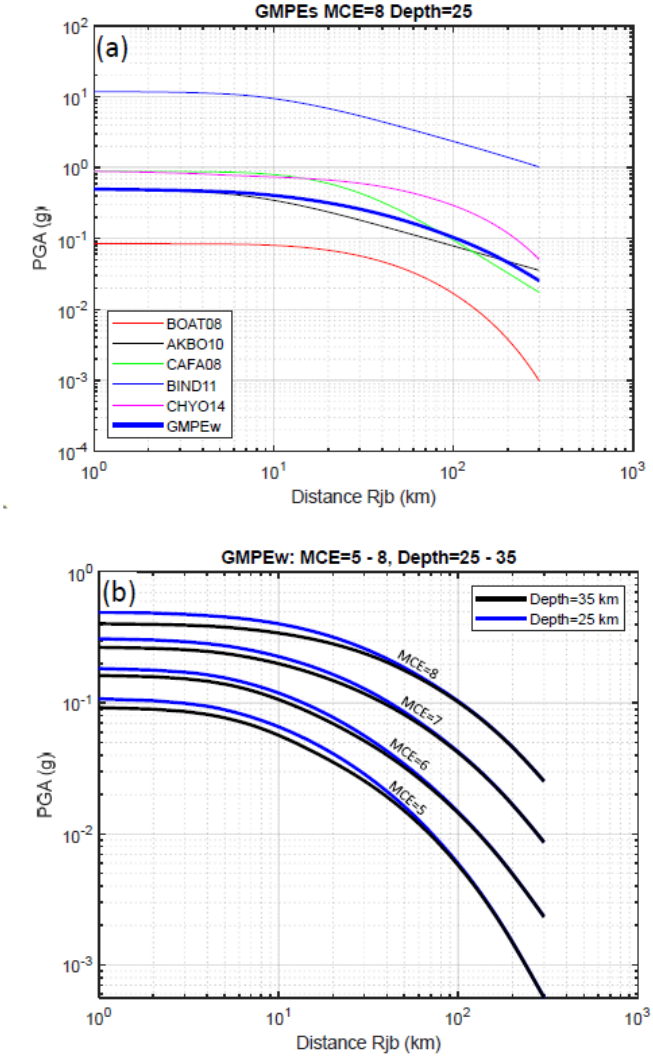

Figure 4. Ground motion prediction equations used and the resulting weighted composition (GMPEw) applied in the DSHA. (a) plot of the different ones: BOAT08, AKBO10, CAFA08, BIND11, and CHYO14 in the case of reverse rupture mode, magnitude 8 and seismogenic source depth 25 km. (b) plots of weighted composition of GMPEs for a magnitude range (MCE 5 to 8), 25 km and 35 km seismogenic source depths, and reverse rupture mode.

ECMs in this work are very close to the upper bound of the low magnitudes used in the Spanish hazard model, so the possible effect of the BIND11 model (Bindi et al., 2011) has been considered with an uncertainty of $\sigma = 0.337$, similar tothe rest of the models, using R_{JB} to obtain log (Y), where Y is in cm/s^2, in rock (V_{s30} > 800 m/s) as a function of the different classes of failure mechanisms. The last of the strong shallow ground motion models used is CHYO14 (Chiou and Youngs, 2014), which obtains Ln(Y), with Y in g in the rock, as a function of the R_{JB} and R_{rup} distances, for which a value of Z_{TOR} =

https://doi.org/10.5194/nhess-2023-52
Preprint. Discussion started: 4 April 2023

40 km has been taken as the upper limit of the mean rupture depth, an average dip of 60º, and the different types of rupture mechanisms that act predominantly in each seismogenic area. In this model,, the random variability includes the magnitude dependence, as long as the threshold of MCE = 5 is exceeded, and the nonlinear response of the ground that has been fitted as a function of V_{s30} (Chiou and Youngs, 2014). Finally, the two models applied in deep areas (Youngs et al., 1997; Zhao et al., 2006) correspond with those of the model developed for Spain, based on subduction data or global databases, applied for seismogenic sources at about 60 km depth, three located S and SW of the Gulf of Cádiz and one E of the Strait of Gibraltar, in the Iberian Peninsula (IGN-UPM, 2017). These models are adaptable for scenarios with high magnitudes (up to Mw 8.5) and long distances with slow attenuations, such as those observed in these areas.

4.2 Deterministic Seismic Hazard Assessment (DSHA)

DSHA was the first methodology proposed in the late 1960s to assess seismic hazard in nuclear power plant design and engineering projects and was later applied to large industrial infrastructures (NRC, 1973; AEIS-IGN, 1979). This method assumes that seismicity behaves stationary by assuming that future earthquakes will occur in a similar way as they did in the past. The simplicity of its application is based on the fact that the seismic information required for its implementation uses geology and seismic history (Krinitzsky, 2005) to identify earthquake sources and interpret the strongest earthquake that each source is capable of producing regardless of time or MCE. Therefore, the DSHA is a method that does not provide information on the return period of the MCE. The MCE earthquake is the largest possible occurrence along a recognised fault under currently known or assumed tectonic activity (USCOLD, 1995), which will cause the most severe consequences at the site.

Since it is based on the maximum effect that can reach the site of an earthquake produced in the area of influence, the most important input parameters are the maximum magnitude associated with the characteristic earthquake as MCE and an attenuation law appropriate to the rupture mechanisms, tectonic regime, validity distance, and transmission characteristics of the wave (e.g., according to V_{s30}), which led to its widespread use for many years (Munuera, 1963; Hays et al., 1975; Arenillas et al., 1982; Panza et al., 1999). For reasons of prudence, and despite the fact that the DSHA does not explicitly incorporate uncertainties through the probability and recurrence functions of seismic events in an area, the seismic hazard can be obtained as a certain percentile of ground motion. It should be noted that although the probability density of the 50th percentile, or average value, is the highest, it is very unlikely that an actual movement will be exactly equal to this estimate. Therefore, in general, the 50th percentile movement is used in preliminary studies with DSHA, and the 84th percentile movement is sometimes used for critical structures. Thus, some deterministic seismic risk analyses use the mean motion plus a design deviation, which is equivalent to an exceedance probability of 16% (Ben-Zion et al., 2003), calculated from simple earthquake and ground motion statistics (Krinitzsky, 1995, 2002) in a particular seismic scenario for which the ground motion risk assessment is based.

https://doi.org/10.5194/nhess-2023-52
Preprint. Discussion started: 4 April 2023


Natural Hazards and Earth System Sciences Discussions

Moreover, depending on how the distribution of seismicity is considered, the application of the DSHA is not zoned, if it is done on a homogeneous seismicity region, with a single seismic source of global influence. On the contrary, if the diversity of seismic behaviour in different seismic areas with local influences is remarkable, the DSHA is zoned and the geometry of each seismogenic source is required for its use. Considering the work on the characterisation of seismogenic structures that has been developed so far and that reveals the enormous variety and heterogeneous spatial distribution, the DSHA used in this work is zoned.

The calculation of the seismic hazard was based on assuming here the occurrence of a large earthquake of a certain magnitude at a specific location that affects the site where the motion assessment is made. For its computation, this work follows a series of steps (Reiter, 1990; Krinitzsky, 1995; Kramer, 1996; Campbell, 2005) that allow the deterministic derivation of the seismic hazard with a zone-based method:

(i) A catalogue construction of N_F seismogenic sources $\{SS_j\}$, which may affect the study area, such an inventory compiles their geometry, depth, and geographic location.

(ii) Characterisation of the seismic potential of each source SS_j that is capable of a significant ground motion at the site for MCE_j and the prevailing focal mechanism (normal, thrust, or strike-slip) of its seismicity.

(iii) For the seismic ground motion intensity parameter Y, by which the hazard is to be characterised, select the set $\{f^i\}$ of the empirical Ground-Motion Prediction Equations (GMPEs) or attenuation laws $Y^i=f^i(M,R,\phi^i_k,\sigma^i_Y)$, with their corresponding parameters ϕ^i_k that include possible dependence on focal mechanism, shear type or S-wave velocity, and the random uncertainties σ^i_Y for each i-th prediction equation.

(iv) Arbitrarily select the desired probability of exceedance $PR_{exed}=Pr[Y>=y_{max}/M,R]$, for a seismic scenario given by the (M,R) pair.

(v) Calculate the p-th percentile equivalent to the probability of exceedance:

$$PC_{Pr}= Pr[Y<y_p/M,R]=1- Pr[Y>=y_p/M,R] \quad (2)$$

(vi) Calculate the standard normal random variable Z_{01}, of mean 0 and variance 1, that matches the percentile PC_{Pr}.

(vii) For a site P located at the geographic coordinate position (x,y,h) with latitude, longitude and hypsometry (height or depth above mean sea level).

(viii) For each j-th seismic source SS_j (j=1,.... N_F), assuming that the worst-case scenario (M,R, focal mechanism) is set, defined as the occurrence of an earthquake of magnitude M=MCEj from a point of the j-th seismogenic source at the shortest possible distance $R = R_{min} =\min\{d(P,SSj)\}$, based on the distance (Fig. 3) to be handled (R_{JB}, R_{ep}, R_{hip}, etc.) in the attenuation function (Fig. 4).

(viii.1) Calculate the mean ground motion (50th percentile or GMPE treated as deterministic) of the seismic parameter $Y^i_{50,j}$ at the site, with each i-th GMPE: $Y^i_{50,j} = f^i(M,R,\phi^i_k)$.

(viii.2) Calculate the p-th percentile of the seismic parameter at the site with the i-th equation of motion:

$$\log Y^i_{p,j} = \log Y^i_{50,j} + Z_{01}\, \sigma^i_Y \quad (3)$$

https://doi.org/10.5194/nhess-2023-52
Preprint. Discussion started: 4 April 2023


Natural Hazards and Earth System Sciences Discussions

(viii.3) Obtain the on-site seismic ground shaking parameter $Y_{p,j}$ on site P produced by each j-th earthquake source.

(ix) Deterministic evaluation of the th percentile of the seismic hazard $Y_p(x,y,h)$ at the site located at (x,y,h) as the largest parameter of the intensity of ground shake obtained from each seismogenic source: $Y_p(x,y,h) = \max\{Y_{p,j}\}$

(x) Write $Y_p(x,y,h)$ output to change to a new location of the P site to assess.

(xi) Repetition of this process at numerous locations spread over a geographical region allows mapping of the hazard assessment over the geographical study area.

Then, as a result we will obtain the estimate of the seismic action on the bedrock of the site studied, which, being a maximum impact value, will be characterised by the most unfavourable seismic scenarios for the seismic ground motion parameter Y. Specifically, according to the formulation of the GMPEs used, the results obtained for Y are PGA (g) in rock, without quantifying the probability associated with the results obtained, although part of the random uncertainties involved in the estimation process have been incorporated in their calculation, as shown above.

The previous hazard estimation is based on the classical deterministic method; however, it is not statistically accurate considering that the intensity of the seismic motion Yp, obtained for a minimum p-percentile, turns out to be the maximum value of a set of independent random variables with a standard distribution function. Since in each GMPE the log Y value is distributed as a normal random variable of mean logY with standard deviation σ (Kramer, 1996), then, since $Y_p(x,y,h) = \max\{Y_{p,j}\}$, both Y_p and $Y_{p,j}$ are random variables. Thus, if the p-th percentile Y_p is calculated as follows:

$$\Pr\left[Y_p <= y_p/M,R\right] = F\left(\frac{\log Y_p - \log y_{max/M,R}}{\sigma}\right) = \frac{p}{100} \quad (4)$$

in accordance with the classical scheme, with a single dominant seismic source, and where F denotes the cumulative density function of the standard normal distribution (e.g., mean μ = 0, and variance = 1). Now, considering the distribution of $Y_{p,NS}$ as the extreme value of a set of values (Coles, 2001; Ang and Tang, 2007), the above approximation is computed as:

$$\Pr\left[Y_{p,NS} <= y_p/M,R\right] = \Pr\left[Y_1 <= y_p/M,R\right] x \Pr\left[Y_2 <= y_p/M,R\right] x \dots x \Pr\left[Y_{NS} <= y_p/M,R\right] = \frac{p}{100} \quad (5)$$

This implies incorporation of the effect of the remaining NS seismic sources in the hazard percentile estimation in the hazard assessment. The estimation is more complicated than in the case of a single source, as it is now necessary to solve the nonlinear equation:

$$\prod_{j=1}^{NS} F\left(\frac{\log Y_{p,NS} - \log y_{j/M,R}}{\sigma}\right) = \frac{p}{100} \quad (6)$$

https://doi.org/10.5194/nhess-2023-52
Preprint. Discussion started: 4 April 2023


Natural Hazards and Earth System Sciences Discussions

As this paper uses an approach based on a logic tree scheme that weights the GMPEs to capture the epistemic uncertainties in the hazard estimation, the above equation is rewritten to solve for each i-th GMPE $f^i(M,R,\phi^i_k)$ used and its corresponding i-th random uncertainty σ^i:

$$\varphi^i\left(\log Y^i_{p,NS}\right) = \prod_{j=1}^{NS} F\left(\frac{\log Y^i_{p,NS} - \log y_{j/M,R}}{\sigma^i}\right) - \frac{p}{100} = 0 \quad (7)$$

from which each $Y^i_{p,NS}$ is obtained.

4.3 Epistemic uncertainty treatment: logic tree scheme in DSHA

There are numerous uncertainties in the SHA methodology that arise from a lack of knowledge or limited understanding of the seismic process. This limited comprehension is due, on the one hand, to the extreme complexity of the process, which hinders its conceptual understanding for its correct modelling, to its irregular spatial and temporal distribution, interfering with the estimation of its frequency distributions, its representation and localisation, the estimation of its sizes, and the definition of the seismic sources. Even after large earthquakes such as the 2011 Tohoku earthquake (Japan), significant ignorance has been revealed in the segmentation of seismic sources and the characterisation of their maximum characteristic earthquake (Stein et al., 2012; Beven et al., 2018). In addition to the lack of precise knowledge of the process that releases seismic energy and how it is transmitted through the geological medium, uncertainties are transferred to the seismicity models that are used, for example, to adjust the models of the GMPEs, whose arbitrary correct choice is itself an uncertain process, of which the statistical adjustment of their coefficients incorporates an estimation error. All these uncertainties, depending on their nature, can be classified as random and epistemic (McGuire and Shedlock, 1981; Kiureghian and Ditlevsen, 2009). Epistemic uncertainty is the scientific uncertainty in the process model, and although it can be reduced with improved knowledge, it is due to gaps in understanding, limited by the complexity of the processes underlying the different elements involved in the seismic hazard. Such gaps may include uncertainties about magnitude frequencies or recurrence rates, parameters of their distributions, maximum magnitudes, rupture mechanisms, consequences and impacts, and the significance of observations in the calibration and evaluation of simulation models. On the other hand, random uncertainty is due to the intrinsic variability due to natural chance, assumed to be irreducible and naturally inherent to the process under consideration. It is parameterised in the parameters involved by probability density functions. These uncertainties influence the hazard estimation and the results obtained, and their quantification has been analysed over time (Toro et al., 1997; Molina Palacios, 1998; McGuire, 2004).

https://doi.org/10.5194/nhess-2023-52
Preprint. Discussion started: 4 April 2023


Natural Hazards and Earth System Sciences Discussions

To predict the representative level of PGA values, it is very necessary to properly select region-specific GMPEs (Bommer et al., 2010). Obtaining specific GMPEs for such tectonically complex regions as the one in this work and in a submerged area by means of strong motion records is very complex. The lack of strong motion records in the study area of this work does not allow for a specific ground motion model at the time of writing, and the usual practice is to select suitable ground motion models for similar or nearby tectonic regimes. Therefore, in this paper, we have used a practical method to incorporate the uncertainties inherent in hazard studies that do not have a GMPE developed specifically for the study region, called the logic tree. The formulation of this method, in which weighting factors are assigned to a particular model based on its likelihood, was done in the late 1980s by Coppersmith and Youngs (1986), EPRI (1987), and National Research Council (1988). The approach of this method, which makes use of many alternative prediction models (Kramer, 1996), can be incorporated into DSHA, which has an advantage over the basic scheme in that epistemic uncertainty is better addressed (Bommer et al., 2005; Bommer and Scherbaum, 2008). To this end, the logic tree is constructed from a series of branches connected through nodes from which the computational process branches according to a possibility or weight, whereby several models can be assigned to each node as different branches with different weights depending on the suitability, importance, or degree of a particular model. To effectively apply the logic tree method, it is essential to select the appropriate weighting factors $\{w^i\}$. The assignment of these weights to the different branches is subjective, based on expert judgement (Budnitz et al., 1997), which relies on the degree of uncertainty of the model, its accuracy, and the expected threshold in the seismic parameter calculated at control sites. Each of the weights $\{w^i\}$ reflect current scientific judgements on the relative merit of alternative models.

In the present study, the epistemic uncertainties have been simplified from a non-probabilistic perspective, considering the joint intervention by weighting the attenuation ratios that are applied to address the seismic ground motion estimation that best fits the known points on the emerged lands: the cities taken as control points and validation according to the PGA values obtained in other SHA studies. In other words, a linear combination model of ground motion prediction equations or attenuation relationships has been used to estimate the PGA in each scenario for each point where it is evaluated.

Specifically, for this work, the composition of the logical tree used in the estimation of the PGA at the site of interest by DSHA, in which different GMPEs are weightedly combined, (Fig. 4b) is the product of the synthesis of the trees proposed by IGN-UPM (2017) and Poggi et al. (2020). The selection of GMPEs to be integrated into the synthesis of the logic tree was carried out by selecting analogues in the source logic trees, as well as those with the highest assigned weight and equally applicable to all seismogenic regions, but considering their particular rupture style. The treatment of uncertainties by the logic tree scheme is made mathematically explicit in the calculation process in the equations to obtain $Y_{p,j}$ at site P produced by each j-th earthquake source:

$$Y_{p,j} = \Sigma_i \, w^i \, Y^i_{p,j}$$

And also to obtain $Y_{p,NS}$ at each site P:

https://doi.org/10.5194/nhess-2023-52
Preprint. Discussion started: 4 April 2023


Natural Hazards and Earth System Sciences Discussions

$$Y_{p,NS} = \Sigma_i \, w^i \, Y^i_{p,NS}$$

which includes the effects of the NS seismic sources. These equations are used when the PGA estimation at the site is based on a single control source with the most unfavourable seismic scenario or where all sources are involved in the PGA estimation according to their particular seismic scenario, respectively.

4.4 Geometric synthesis of seismogenic zonings

To integrate the ZESIS and NAF models of seismic zonation, which have been selected here to form the new model of seismogenic sources used as input parameter in the calculation of the seismic hazard in our study area, their compatibility was determined through the previous analysis of the seismic catalogue used and the type of seismogenic sources used to characterise the distribution of seismicity (areal, point or fault type) in each one of them. The selection of the areal seismogenic sources from each zoning was made by taking those that, intersecting with the study area, contribute, either by proximity or by maximum magnitude, to the seismicity of the studied area. The seismic influence area was established within a buffer of 300 km (US NRC, 1997) from the study area (Fig. 5a). Additionally, some seismogenic sources adjacent to the area of seismic influence were selected, and their effect was quantitatively studied. Their seismic contribution was analysed by comparing the results of ground-motion intensities obtained from the DSHA of models with and without the use of these sources.

The overlapping between seismogenic sources, generated from the synthesis process of both zonings (ZESIS and NAF), which can cause the amplification of the seismic contribution in some areas due to the superposition of sources, was treated by means of a topological adjustment. This operation allowed geometric adjustment without overlap between the seismogenic sources, located mainly at the boundaries of the ZESIS and NAF models used (Fig. 5b), considering the seismotectonic considerations that control their boundaries and that are included in the models. As each seismogenic source has associated seismic parameters, the result of the origin zonings, these have also been considered in the synthesis process to create the joint zonation, harmonising the seismicity contributed by the seismogenic sources to the study region, as was carried out in the zonations resulting from the IBERFAULT, OPPEL, and SISMOGEN projects (García Mayordomo, 2015) to calculate the seismic hazard in the Iberian Peninsula. Furthermore, the procedure is supported by recent models for classification and segmentation of tectonic regions using fuzzy logic (Chen et al., 2018). This model is specifically designed for a seismic hazard analysis context based on the geophysical characteristics of the crust, including seismic moment release, seismic anelastic attenuation, and shear wave velocity variations. The tectonic similarity of the area addressed in this work is shown, as it presents similar characteristics in almost all its extensions in terms of the scale of the seismic source and the propagation of seismic waves. However, since this is a work on a global scale, more local studies can also be considered (Vilanova, 2018).

https://doi.org/10.5194/nhess-2023-52
Preprint. Discussion started: 4 April 2023

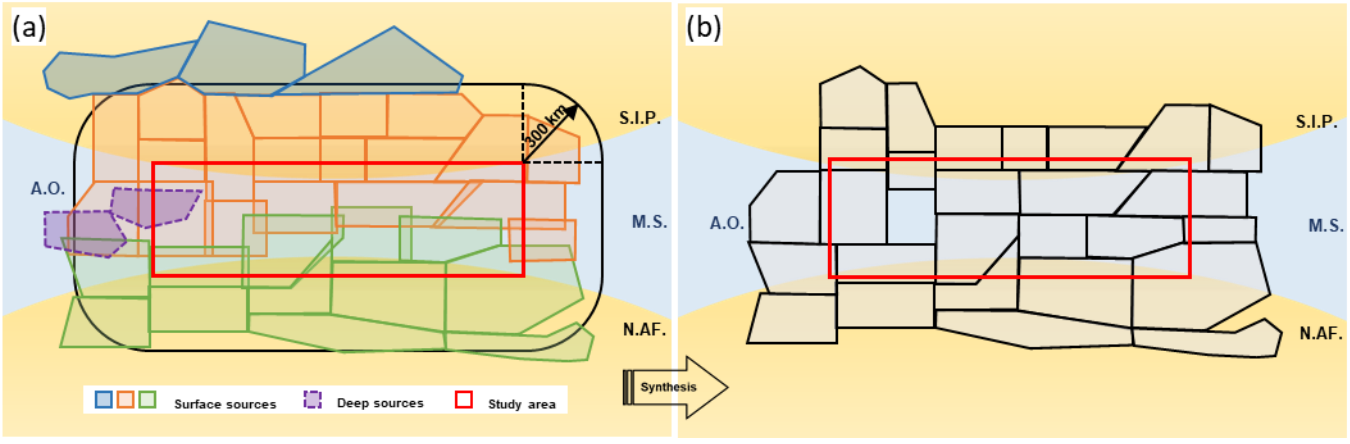

Figure 5. Graphical sketch of: (a) Initial schematic distribution of subsurface and deep seismogenic sources around the study area between the southern Iberian Peninsula (S.I.P.), north Africa (N.AF.), the Atlantic Ocean (A.O.) and the Mediterranean Sea (M.S.), and (b) mapping resulting from the synthesis and integration of seismogenic source zonation from the previous ones.

Once the synthesis of zones has been carried out and the catalogue of sources to be studied in the area has been prepared for its application in the evaluation by means of DSHA, it is necessary to assign a seismic characteristic to each of them, thus completing the inventory. The deterministic method that has been applied, being an extended version to 2.5D, since the value of the hazard on the earth's surface is evaluated taking into account the spatial position of the site (Long. X, Lat. Y, elevation Z) and the position of the source demands as geometric information of the source, in addition to its geometry, which is detailed by the geographical location of the vertices of the polygonal that delimits it, the average depth at which the seismicity is found. It also specifies its rupture mechanism and the characterisation of its seismic potential by means of the MCE.

The geometry of the sources has been obtained from the information provided in open access from the ZESIS website maintained by IGME-CSIC (https://info.igme.es/zesis/, last visited 15/02/2023) and from the GEM Foundation website in its version v2018.0.0 (2018-12-05, https://hazard.openquake.org/gem/models/NAF/, and https://platform.openquake.org/documents/261, last visited 15/02/2023) by downloading the shp files from both databases. The assigned depths for each source will be extracted from the information provided by both bibliographic references (downloaded files for ZESIS from https://info.igme.es/zesis/, and Fig. 7 for NAF, Poggi et al., 2020), as well as their corresponding predominant rupture mechanisms (as normal, reverse, or strike-slip). The MCE values, as the seismic characteristic of each seismogenic source, are used in the GMPEs to estimate the PGA values, setting the seismic scenario (M,R) at the selected grid point or site. Therefore, the estimation of the MCE in a SHA becomes indispensable as it reflects the maximum energy capacity that can be released in an earthquake. In practice, the value of the MCE for a given source in the synthesis zoning is determined by the level of information available. Usually the MCE does not correspond to the largest magnitude earthquake on the nearest major fault. When there is insufficient geological information, the MCE is estimated by

https://doi.org/10.5194/nhess-2023-52
Preprint. Discussion started: 4 April 2023

slightly increasing the historical maximum, e.g., by one degree in intensity or half a degree in magnitude, although this increase depends on the seismic potential of the area (as Poggi et al. 2020 have done in NAF). The expected upper limit of the seismic magnitude that can be generated by a source is considered to be the maximum expected MCE or magnitude of that source, assuming that no source will cause an earthquake of magnitude greater than this (Joshi and Sharma, 2008). Therefore, the values of the MCEs used in this work for each source resulting from the synthesis have been extracted from the ZESIS (MMmax in Table 10; IGN-UPM, 2017) and NAF (Mmax in Table 7; Poggi et al., 2020) zonings. Although MMmax and Mmax are very similar values or for many sources the same, in others they present slight differences, so MCE = max $\{MM_{max}, M^{max}\}$ has been taken.

4.5 DSHA calculation specifications

The computer-programmed DSHA method can be found in the literature in various forms to perform the calculations efficiently over a geographical area, with its particular ground motion and seismotectonic characteristics. Published versions range from those that adapt their programming with Excel to the particular case studied (Loi et al., 2018), or in Igor Pro (Huang and Wang, 2012). Others, with a more general scope of application, are programmed on a computational system such as MATLAB (Vipin, 2013; Candia et al., 2019; Ramkrishnan et al., 2021), or with a high-level programming language such as FORTRAN. There are also specific programmes for SHA, such as Shakemap (Worden et al., 2020) in which BMKG (Badan Meteorologi, Klimatologi, dan Geofisika) modified in 2015 to incorporate DSHA (Zulkifli et al., 2017). Of these, in this paper an open source Visual Basic (VBA) script in Excel (Wang et al., 2012), which has been used in other studies from a deterministic perspective (Wang and Huang, 2014), has been selected for DSHA evaluation. Originally, the algorithm of this script is designed to perform standard deterministic hazard calculations on a given geographic coordinate location, and its input interface allows the incorporation of multiple linear or polygonal seismogenic sources, their seismic characterisation according to the MCE, and the calculation of the seismic hazard map by the deterministic method, by reproducing the same calculation that is done on a point on a grid of geographic coordinate data points.

As it is a programme built on a commonly used software tool for data analysis such as Excel and written in VBA, it uses an intuitive and easily arranged spreadsheet as the data input interface for the computation and output of results, which makes it a more user-friendly tool than other programmes written in high-level languages. The results obtained are given as PGA, PGV, or PGD values, according to the seismic parameter collected in the ground motion functions. The calculation performed at one point can be repeated on a geographical grid of points, which can then be spatially represented as hazard maps for the parameter in the study area. For the estimation of the DSHA, the study region in this work was incorporated as a grid of calculation points composed of 4,143 sites (Fig. 6a), separated by 0.1 degrees of latitude and longitude, equivalent to approximately 10 km. This grid size was chosen on the basis of experience and approximately equal to the standard error in earthquake epicentre determination (Panza et al., 1990; Suhadolc, 1990). Each point on the grid is considered an individual site. The PGA values in rock have been obtained at all grid points, following the standard DSHA procedure

https://doi.org/10.5194/nhess-2023-52
Preprint. Discussion started: 4 April 2023

provided by Kramer (1996) and Villaverde (2009) with the improved calculation specifications given in the following. Once the PGA values for each grid point have been estimated, they are compiled into a single catalogue showing each grid point in latitude and longitude and the PGA value associated with that particular point. This file is then used to generate seismic hazard contour maps of the study area using 2D representation software.

The internal programming of the Excel script has been modified by editing the macro programmed in VBA, which allows the programme to be configured with the parameters of a new study, or to make modifications to extend the capabilities of the SHA calculation code. In this sense, the original script has been modified in the first phase to programme a series of user-defined functions and VBA subroutines that incorporate each of the GMPE that have been taken as attenuation functions for the study area and the logical tree scheme to weights them. When transferring the 2D flat calculation to a 3D space in which the sites where their hazard is assessed are located on a DTM adapted to the mesh size on which the DSHA is performed (Fig. 6a), each source has been assumed to be horizontally distributed at its corresponding depth (Table 1) and the distances (disregarding the curvature of the earth for the dimension of the study area) involved in the formulation of each GMPE (Rx, RJB, Rrup) must be reformulated appropriately for their correct calculation. To adapt the calculation with the correct 3D distances, it has been adapted using Haversine approximations to the distance on the great circle (on the basis of a spherical earth, i.e., ignoring ellipsoidal effects which is accurate enough for this paper purpose), the depth of the seismogenic source, and the elevation (altimetric or bathymetric) of the point where the evaluation is being carried out, with the minimum distance calculated with the original Scritp. Furthermore, some of the ground motion functions are specific to a type of rupture in the source that causes the shaking, so it has been necessary to include this information in the seismic characteristics of each source that are detailed in the spreadsheet for data entry.

To account for uncertainty in ground motion models, this article has evaluated the effect on DSHA by choosing two values of 16% and 2% of the desired exceedance probability above the mean $PR_{exed}=Pr[Y>y_{max}/M,R]$, for a seismic scenario. In DSHA, the 84th percentile movement to one standard deviation above the mean is usually adopted (Bommer, 2003), instead of the 50th percentile (mean movement). The 98th percentile has also been obtained corresponding to the probability of exceedance probability $\underline{Pr}[Y<=y_{max}/M,R]$, in addition to the usual 50% or mean movement of the ground.

The calculations performed above make it possible to obtain the value of the estimated hazard at the site caused by the seismic effect of a single source whose seismic scenario is the most adverse for the conditions of distance and magnitude, discarding the possible coupled effect which, although minor, could be contributed by the rest of the sources whose scenarios are less hazardous. Therefore, to assess the hazard for a specific exceedance probability, considering the scenario in which all seismic sources contribute (maximum Y distribution) and with a logic tree approach (unlike the one used by Wang and Huang (2014), which only work with one GMPE) a subroutine has been included in the program that solves the nonlinear equation lineal $\varphi^{i}\left(\log Y^{i}_{p,NS}\right) = 0$ by means of a numerical Bisection method, also known as halving, binary search, dichotomy or Bolzano (Atkinson, 1991; Süli and Mayers, 2003). This numerical approximation method, as the binary search

https://doi.org/10.5194/nhess-2023-52
Preprint. Discussion started: 4 April 2023


Natural Hazards and Earth System Sciences Discussions

algorithms popularly used in computer science (Knuth, 1998), is very robust, since it takes advantage of a corollary of the intermediate value theorem. The classical Bolzano theorem or the intermediate value theorem ensures that a continuous function that changes sign in an interval has a root. In our case, the continuous function $\varphi^i(x)$, if the values of $\varphi^i(a)$ and $\varphi^i(b)$ have opposite signs, at least exist one value $x^* \in (a,b)$ or root of φ^i, such that $\varphi^i(x^*) = 0$. Using as initial search interval (a,b) = $(\min\{ \log y_{j/M,R}\}, \max\{ \log y_{j/M,R}\}+3\sigma^i)$, within it is verified that the Bolzano condition is fulfilled: $\varphi^i(a)\ \varphi^i(b) < 0$, the process of the bisection method process has been carried out to approximate numerically this root ($Xo \rightarrow X^*$):

Calculate Xo=(a+b)/2
If $\varphi^i(a)\ \varphi^i(Xo) <0$, the root $X^* \in (a,Xo)$, then
    assign b=Xo
Else If $\varphi^i(Xo)\ \varphi^i(b) <0$, the root $X^* \in (Xo,b)$, then
    assign a = Xo
End if
Back to calculate Xo

Since this process must be repeated at each site where the hazard is estimated and, in this case, for each GMPE, the convergence characteristics of this algorithm allow it to be repeated for a total of 100 iterations, which are sufficient to achieve an admissible error |Xo - X*| in the root X* solution of the equation (Burden et al., 2015):

$$|Xo - X^*| \leq |b - a|\ 2^{-100} \quad (8)$$

The robustness of this method guarantees convergence without complex operations, although it is slower than other iterative numerical methods for solving non-linear equations (Hamming and Hamming, 1986). In addition, this technique has a guaranteed error bound, which is reduced by 12% with each iteration. To represent the new calculations made from the script with the above modifications, it has been necessary to adapt not only the input of new data (DTM, depth, rupture mode of the seismic sources, random error of the GMPEs, etc.), but also the output of results in the VBA script and its graphical representation has been tailored to represent the effects with the distance of each source and for various exceedance probabilities. In addition to providing the DSHA map, the output has been customized to represent the site effect of each source with distance from a particular site with its 3D location (longitude, latitude, and elevation) and to assess the joint or similar effect of sources, detect the most influential ones, and for a particular site study could determine the effect of its seismogenic zones in the worst-case scenario separately or together with DSHA (Sá et al., 2021).

4.6 Sensitivity and comparative analyses

The results obtained with the DSHA method implemented in this work may be significantly affected by the incorporation of the DTM, as some of the GMPEs, incorporated in the logic tree scheme, use a 3D distance metric in their

https://doi.org/10.5194/nhess-2023-52
Preprint. Discussion started: 4 April 2023

Natural Hazards and Earth System Sciences Discussions

set of independent variables (e.g., Rrup or Ry). Typically, the DSHA is planimetric, and 2D distances are evaluated on a horizontal plane and does not use 3D distances to deep sources from the DTM sites, as has been done here. These distances act on the hazard result by defining the seismic scenario affecting each point, and this is used on the set of GMPEs to evaluate the seismic acceleration of the PGA terrain. Likewise, the GMPEs used incorporate certain particularities that are applied according to the type of rupture, so that the result of considering the same style in all the sources may give rise to disparate results than if the specific predominant style of each source is used. In order to assess the sensitivity of the results to the effect of using the DTM and incorporating the information of the rupture style in each source, a descriptive statistical study has been carried out with parametric and nonparametric probabilistic methods on the resulting PGA maps and their absolute differences. With the difference maps, it is possible to identify and contrast the areas with similar behaviour in all cases, or with little sensitivity to the TDM effect and type of rupture, or to detect areas with abnormally high PGA outliers.

The quality of the PGA map obtained by incorporating the DTM and the typology of the breakdown of each source has been assessed through two comparison criteria. 1) The geographical distribution of PGA values (g) with that obtained and published in four PGA maps (EHSM13-SHARE: Woessner et al. (2015); zoned PSHA: IGN-UPM (2017); unzoned PSHA: Crespo et al. (2014); and NAF zoned PSHA: Poggi et al. (2020)) that partially cover the study area. 2) Comparing the average PGA values (50% percentile) obtained from the calculation with the model presented here in nine cities (Fig. 6a) uniformly distributed throughout the study area and for which six previous studies have published their calculated values (Table 1) of the PGA hazard (Crespo et al., 2014; Rivas Medina, 2014; Salgado Gálvez et al., 2015; Woessner et al., 2015; IGN-UPM, 2017; Poggi et al., 2020).

Table 1: Estimated PGA values (in g) presented from various authors (Annex VI in IGN-UPM (2017), NAF (Poggi et al. 2020), EHSM13-SHARE (Woessner et al., 2015), Crespo et al. (2014), Rivas Medina (2014) and CIMNE (Salgado Gálvez et al., 2015)) in each city used to control the results obtained from the DSHA calculation in the study area.

Main Region	City	Lat.	Long.	IGN-UPM	NAF	EHSM13 SHARE	Crespo	Rivas Medina	CIMNE
Southern Iberian Peninsula	Cádiz	36.533	-6.295	0.11	-	0.10	-	-	-
	Málaga	36.717	-4.424	0.16	-	0.11	-	0.20	-
	Almería	36.836	-2.464	0.19	-	0.13	-	0.30	-
	Huelva	37.267	-6.950	0.12	-	0.13	0.11	-	-
	Granada	37.183	-3.583	0.23	-	0.17	0.30	0.30	0.19
	Alicante	38.200	-0.483	0.18	-	0.11	0.22	0.25	-
North Africa	Tánger	35.791	-5.829	-	0.18	-	-	-	-
	Melilla	35.294	-2.936	-	0.24	-	-	-	-
	Orán	35.708	-0.637	-	0.32	-	-	-	-

https://doi.org/10.5194/nhess-2023-52
Preprint. Discussion started: 4 April 2023


Natural Hazards and Earth System Sciences Discussions

Incorporating uncertainty in the ground motion models, this work has evaluated the effect on the DSHA of choosing two values of 16% and 2% of the desired exceedance probability above the mean, which translates into an effect on the spatial and statistical distribution of the PGA map values, which have also been analysed from a descriptive statistical perspective. The consideration of different levels of uncertainty also affects the results obtained for the set of cities used as control ground motion values and how the control scenario varies in each of them and the rest of the scenarios with distance.

It is possible that in some of the 4,143 sites (Fig. 6a), over which the seismic movement is evaluated to construct the PGA map, the control scenario could be composed of several sources, not easily distinguishable if their uncertainty is considered. For this reason, the results obtained with the DSHA method, in which all seismic scenarios are used to evaluate, according to their random uncertainty, the different percentiles of the PGA, have also been contrasted by means of descriptive statistics, facilitating their comparison with the rest of the results in the previous cases.

5. Results

5.1 Seismic zonation

As a previous result to carry out the seismic hazard analysis in this work, a new seismic zonation of areal seismogenic sources was generated, synthesis of the integration of the described ZESIS and NAF models. For this new zonation, 39 seismogenic sources were initially considered, of which 35 were those that formed the final zonation (Fig. 6b to d). This new zoning incorporates the sources from the NAF to the south and the ZESIS sources within and surrounding the study area. The ZESIS sources to the north (9 to 12, Table 1), on the Iberian crust, have been discarded because of their deep (about 30 km) and low influence at the distances marked by the 300 km buffer around it. The four deep sources located in the south and southwest of the Iberian Peninsula (between 40 and 65 km depth) were discarded, as their effect is negligible compared to the scenario of the rest of the ASCR sources at shallower depths and with a higher sympathetic intensity. The depths at which these sources are located vary between 20 and 36 km (Fig. 6b). The seismic characteristics derived from the ASCR seismogenic sources have maximum magnitudes (MCE) ranging from 6.2 to 8.9 (Fig. 6c), where a clear relationship is observed between the zones of higher magnitude and the zones of higher instrumental seismicity. The predominant rupture mechanism is inverse in the band from the Gulf of Cádiz towards the Algerian Mediterranean coast, passing through the southern Rif and running parallel to the Atlas chain (Fig. 6d), which is the characteristic rupture mode in areas of plate collision where large compressive stresses act, as in the case of our study region. This mechanism reorganises in the form of shearing toward the Alboran Sea basin and the coastal area of the Iberian Peninsula and towards the interior of the Iberian Peninsula it becomes more extensive with a normal structure.

The catalogue thus constructed contains, in addition to the geometry of the zonation, the seismic parameters of each source necessary for the DSHA calculation (Table 2). The MCE and the style of the predominant rupture mechanism in each zone according to the focal mechanisms analysed in the original ZESIS and NAF catalogues. The depth in kilometres has

https://doi.org/10.5194/nhess-2023-52
Preprint. Discussion started: 4 April 2023

been calculated as the average of the depth range given in the seismic record for each source. The shallowest depth values are found in the 17 km of zones 40 and 41, (Table 2) in the western Alboran Sea (40), in the Betic crust that borders the Gibraltar Arc, and in the Algerian-Balearic basin, in the oceanic crust at the eastern edge of the study area (41). Both are predominantly driven by a transpressional shearing mechanism with NNW-SSE shortening direction resulting in moderate (40) to low (41) activity, with magnitudes slightly below 7. The deepest sources within the SACR are distributed over the emerged margin of the Baetic and its connection with the Rif through the Gibraltar Arc, at depths ranging from 33 km to 36 km, subjected to a strike-slip regime that becomes extensive toward the interior of the Iberian Peninsula (Fig. 7d) and with ECM magnitudes between 7 and 7.5. Most of the shallower sources, with depths of less than 23 km, are distributed on the southern border of the study area (sources 52 and 3 to 9), beneath the Atlas Mountains. These sources have been included in the catalogue because, although they have relatively low MCEs, they are close enough to the sites to contribute to their hazard. The remaining sources are located at intermediate depths around 26 km, between 23 and 30 km, in mainly rifting and reverse regimes. Notable among these sources are source 50, on the Gorringe submarine relief and the northern half of the Horseshoe Abyssal Plain, on the western edge of the study area, with an MCE of 8.9, and the sequence of 45 to 47 on the Arzew and Yousuf faults, off the Algerian coast, with an MCE of 7.9 to 8.1, all subject to a compressive stress regime with NNW-SSE directions of maximum shortening.

5.2 Seismic hazard maps, sensitivity and quality

The PGA (g) seismic hazard maps for the MCE, considering the maximum control scenario in each of the 4,143 points used to obtain the map, have been obtained without the DTM, taking each point of the map at 0 m elevation and the ASC seismogenic sources with a single rupture mechanism to tear for all of them (Fig. 7a) and assigning to each source its particular rupture mechanism (Table 1) (Fig. 7b). The maximum calculated PGA values are close to 0.83 g in both cases (PGA(0,reverse) and PGA(0,RM) in Fig. 7c), although the 75th, 50th and 25th percentiles are somewhat lower, in the case of the latter case assigning each source its particular rupture style, with a mean PGA (PGA_{50}) of 0.317 g, as compared with 0.297 g. However, if each point on the map is assigned its corresponding elevation according to the GEBCO DTM (Fig. 1), the maps obtained (Fig. 7d and 7e) show very modest relief influence and have values slightly higher than the two previous ones without DTM of 1.1 g in both cases (PGA(H,reverse) and PGA(H,RM) in Fig. 7c), although they do show higher percentile values than the two previous cases, with an average PGA of 0.331 g and 0.30 g, respectively. In the four cases presented, the highest PGA values are located on the Gorringe submarine relief up to the Horseshoe plain, areas affected by sources 50 and 52, of moderate to strong seismicity and values in the range of the PGA distribution outliers in the area, approximately 0.6 g to 0.85 g without DTM and within the values of 0.65 g to 1.1 g with DTM. To the west, the sequence of sources 44 to 47 of moderate seismicity in the Algerian coastal zone in the area of the Arzew faults show values of 0.46 to 0.51 g without DTM, and 0.47 g to 0.54 with DTM. In the case of using a single rupture style, the PGA values show a smooth transition from N to S in the Alboran Sea basin area (Fig. 7a and 7d), however, when the style specific to each source is applied, this transition is more abrupt (Fig. 7b and e).

https://doi.org/10.5194/nhess-2023-52
Preprint. Discussion started: 4 April 2023

Natural Hazards and Earth System Sciences
Discussions

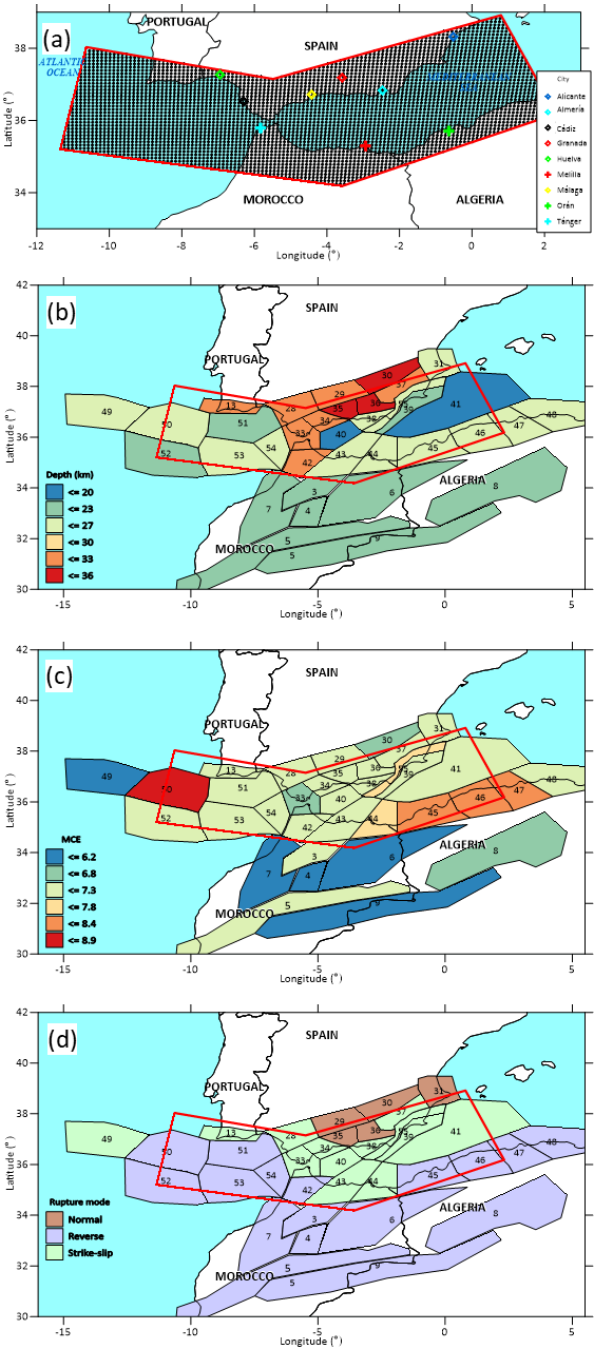

Figure 6. (a) Mesh of 4,143 points with 0.1º spacing on which the DSHA calculation has been performed. The nine cities used for the validation of results have been marked. Sinthesis of the seismogenic source zonation considered in this work for DSHA evaluation on each (a) point, in both South Iberia and North Africa regions and the parameters geographical distribution (Table 1) used in GMNAFI model for DSHA estimation: (b) depth (km), (c) magnitude of máximum considered earthquake (MCE), and (d) main rupture mode for each seismogenic source.

https://doi.org/10.5194/nhess-2023-52
Preprint. Discussion started: 4 April 2023

Natural Hazards and Earth System Sciences
Discussions

Table 2: Denomination of the seismogenic sources and their seismicicity parameters extracted from ZESIS (IGN-UPM, 2017) and NAF (Poggi et al., 2020) zoning models, used for the construction of the synthesis seismogenic model with which the DSHA has been calculated in the study area. The mean value MMmean, standard deviation sMM and minimum MMmin and maximum truncation limits MMmax, are parameters of the maximum magnitude (MCE) distribution.

Main Region	Source No. Id.	Rupture Mechanism	Depth (km)	MCE Distribution			
				$<M_{max}>$	σMM	Max_{min}	$M_{máx}$
Southern Iberian Peninsula **ZESIS**	**13**	Strike-slip	31.0	6.5	0.2	6.0	6.9
	28	Strike-slip	31.0	6.7	0.2	6.3	6.9
	29	Normal	31.0	6.6	0.4	6.2	6.9
	30	Normal	33.0	5.0	0.4	4.6	6.3
	31	Normal	25.0	6.6	0.4	6.5	7.1
	33	Strike-slip	30.0	5.8	0.4	5.4	6.4
	34	Strike-slip	30.0	6.6	0.3	6.3	7.0
	35	Normal	33.0	6.8	0.3	6.5	7.1
	36	Normal	36.0	6.6	0.4	6.2	7.0
	37	Strike-slip	32.0	6.8	0.2	5.4	7.0
	38	Strike-slip	24.0	6.7	0.2	6.5	6.9
	39	Strike-slip	22.0	6.7	0.1	4.9	6.9
	40	Strike-slip	17.0	6.5	0.3	6.0	6.8
	41	Strike-slip	17.0	6.5	0.4	4.7	6.9
	42	Reverse	30.0	6.8	0.3	6.5	7.1
	43	Strike-slip	25.0	7.0	0.2	6.2	7.3
	44	Strike-slip	24.0	6.4	0.4	6.0	7.4
	45	Reverse	26.0	7.3	0.5	6.8	7.9
	46	Reverse	26.0	7.5	0.3	7.2	7.9
	47	Reverse	26.0	7.6	0.4	7.3	8.1
	48	Reverse	26.0	6.8	0.1	6.6	7.1
	49	Strike-slip	24.0	6.0	0.1	5.9	6.2
	50	Reverse	26.0	8.7	0.2	8.5	8.9
	51	Reverse	23.0	6.8	0.3	6.6	7.1
	52	Reverse	23.0	6.4	0.2	6.2	7.1
	53	Reverse	24.0	5.7	0.2	5.5	7.0
	54	Reverse	24.0	6.9	0.4	6.5	7.3
	55	Strike-slip	25.0	6.7	0.3	6.6	7.4
	9	Reverse	26.0	6.8	0.3	6.5	7.2
	10	Reverse	31.0	6.3	0.3	5.7	6.8
	11	Reverse	30.0	6.1	0.2	5.9	6.3
	12	Strike-slip	31.0	5.1	0.3	4.9	6.4
North Africa **NAF**	**3**	Reverse	22.0	6.7	0.5	-	7.2
	4	Reverse	22.0	5.2	0.5	-	5.7
	5	Reverse	22.0	6.4	0.5	-	6.9
	6	Reverse	22.0	5.3	0.5	-	5.8
	7	Reverse	22.0	5.5	0.5	-	6.0
	8	Reverse	22.0	5.8	0.5	-	6.3
	9	Reverse	22.0	5.61	0.5	-	6.11

https://doi.org/10.5194/nhess-2023-52
Preprint. Discussion started: 4 April 2023

Natural Hazards and Earth System Sciences
Discussions

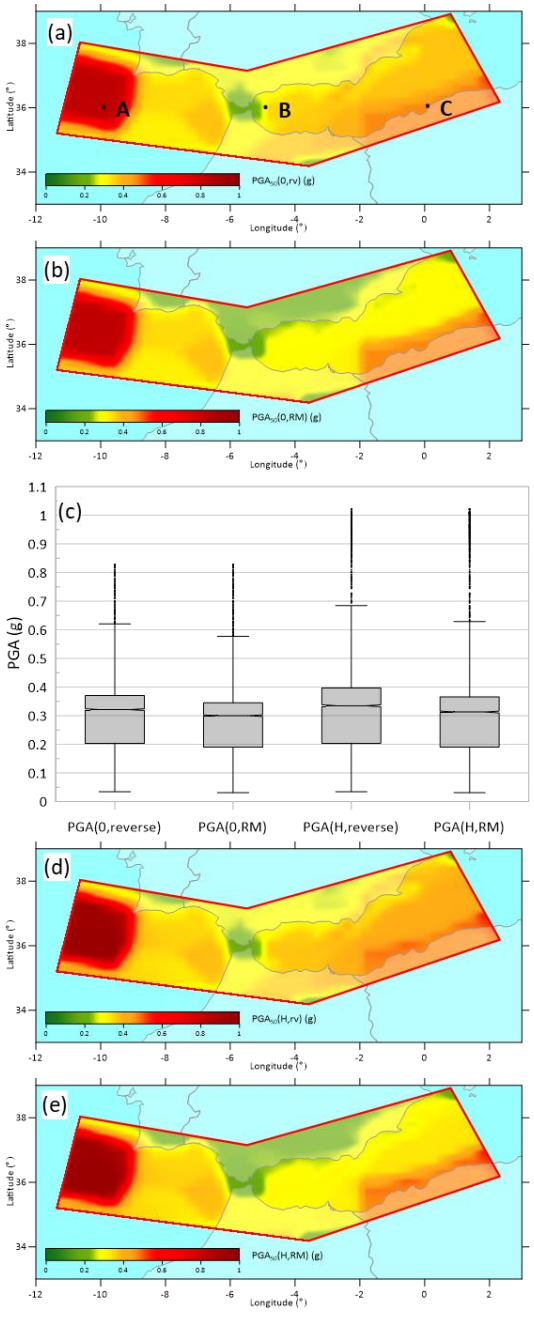

765 **Figure 7.** PGA maps (in g) obtained with the DSHA method in this work: (a) without DTM and considering only a reverse focal mechanism in all seismogenic sources; (b) without DTM and considering a source-specific average focal mechanism (Table 2). (c) Box-Whisker plots fo PGA values used for Figures 7a,b,d, and e. Center line represents the mean value. Box edges are limited by the quartiles (25% lower and 75% upper percentile). Whiskers are limited by the 1.5 times the inter-quartile range. The notch size factor is 1.7. The sample outliers are represented by dot symbols. PGA maps (in g) form DSHA: (d) with DTM (Figure 1) and considering a reverse focal
770 mechanism in all seismogenic sources; (e) with DTM (Figure 1) and considering a source-specific average focal mechanism (Table 2).

https://doi.org/10.5194/nhess-2023-52
Preprint. Discussion started: 4 April 2023

Natural Hazards and Earth System Sciences
Discussions

The behaviour at three points in the region (A, B, and C in Fig. 7a), located in areas with different seismic conditions: one in the Gorringe area (10ºW, 36ºN), one in the Gibraltar Arc area (5ºW, 36ºN), and one in the Algerian coastal area (0ºE, 36ºN), versus the effects of incorporating the DTM in the calculation (Fig. 8a), produce appreciably different increases in ground motion depending on the intensity of the seismicity in which they are located, for the same range of variability in their elevation, evaluated from 1000 m above sea level to 4000 m depth. The point over the Gorringe area suffers an increase of up to 17.5% between the PGA obtained at 0 m (0.828 g) and that which would be obtained if the point were at -4000 m depth (0.970 g). This increase is reduced to 12.1% for the point in the Algerian area, and in the Gibraltar Arc area it is reduced to 10.1%. The rate of change and increase of the PGA, as the distance to the control source varies, in the three cases

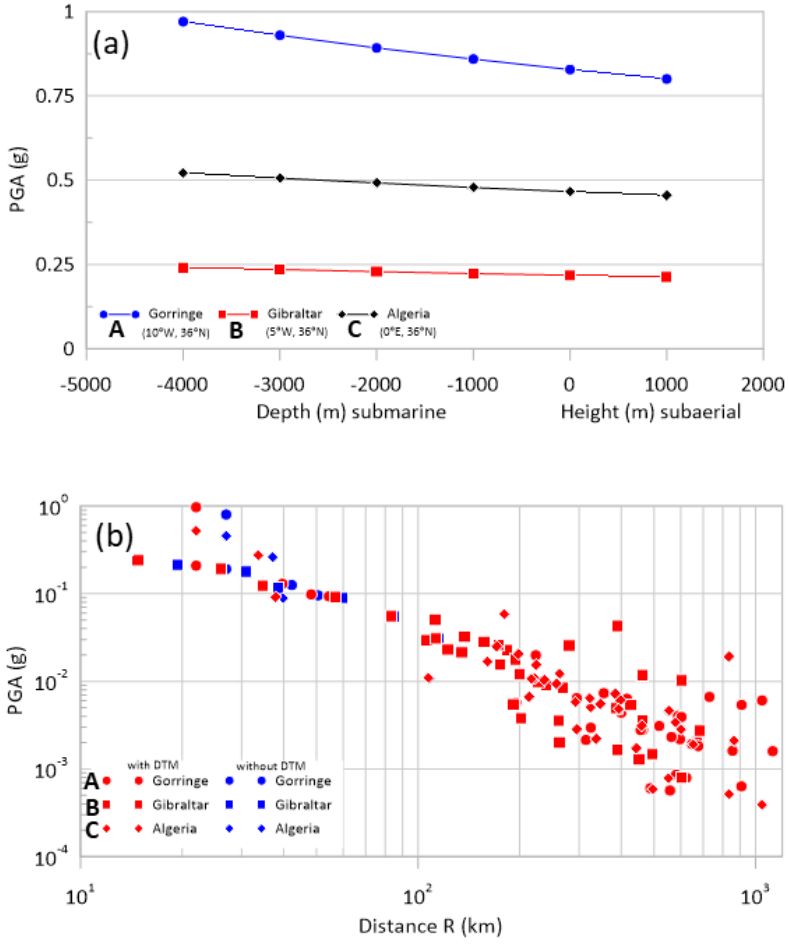

Figure 8. Effect of the DTM on the values obtained at three points distributed in the study area (Figure 7a): A Gorringe (10ºW, 36ºN), B Gibraltar Arc (5ºW, 36ºN), and C Algeria coast (0ºE, 36ºN), (e) considering that the points (A, B, and C) are at different elevations: between 1000 m and -4000 m, and (f) according to the control earthquake of every source on each point (A, B, and C), considering that the points are at 0 m (red symbols, with DTM) and at -4000 m (blue symbols, without DTM).

https://doi.org/10.5194/nhess-2023-52
Preprint. Discussion started: 4 April 2023

shown, has a practically negligible change, almost constant, for the range of elevations analysed. The individualised effect of each source on this behaviour for the extreme cases of elevation 0 m and -4000 m has been represented (Fig. 8b) according to its control earthquake and the distance R at which the source is located considering its depth. In this graph it is possible to recognise how up to 100 km distance there is an appreciable effect on the PGA value, higher than 0.1 g and up to 100 km distance. After 100 km, the difference in the PGA obtained using the DTM and without it is less than 1%. The effect on the three points, which have been taken over areas of different simian intensity, is more noticeable at 0.1 g and above, with the five seismic sources closer to the site, and attenuates to almost zero at 100 km and above.

The spatial distribution of this behaviour is shown by the differences between the previous maps (Fig. 9a, 9b, 9d, and 9e) and their distribution statistics (Fig. 9c). The differences in the PGA obtained with and without DTM, and in the same conditions applied for the calculation according to the case of the rupture mechanism (reverse only, Fig. 9a: PGA(H,reverse)-PGA(0,reverse) and source-specific rupture mode, Fig. 9c: PGA(H,RM)-PGA(0,RM)), show that, regardless of whether DTM is used or not, the most important differences between assigning or not a predominant rupture mechanism in the whole area or the specific one in each seismogenic source are less than 0. 2 g (Fig. 9c). The positive increases observed over the reference values calculated without using the DTM (red tones) are areas of the map whose depth is closer to the source, being more intense in the deeper oceanic zones. In other words, in the areas of the submarine domain, the PGA values obtained are higher if the DTM is used, being the highest in the areas with the highest PGA values (Gorringe, Horseshoe and Coral Patch areas). The differences are negative (blue shades) in the surfaced areas, although lower than the positive ones (they are below 0.01 g) show that the PGA value obtained using the DTM is lower than that obtained without using it. The differences between using a common rupture mechanism according to the predominant one and the specific one of each source do not exceed 0.08 g (Fig. 9b: PGA(0,reverse)-PGA(0,RM) and Fig. 9d: PGA(H,reverse)-PGA(H,RM), being null the difference in the areas where the specific mechanism coincides with the reverse one used and highlighting the difference of 0. 7 to 0.8 g in the extensional rupture zones (NE of the Betic) and with a moderate difference of 0.05 to 0.07 g in the rifting zones distributed in the Alboran basin and East of the Rif.

The results obtained for PGA (g) in the nine selected point-cities (Table 1) show variations according to the parameters specified for their calculation on the assignment of the rupture mode and the use of the DTM in the calculation (columns DSHA1 to DSHA4 in Table 3). Some cities show important variations between the different calculation options of up to 31% in Granada, others show no variation in the calculated PGA, such as Huelva or Orán, although most of them are between 20.8% in Málaga and 23% in Almeria. The values obtained with the DSHA methodology used in this work show values higher than those obtained with the probabilistic methodology. Some of them are twice as high as those obtained with PSHA in some previous studies, and the differences are reduced in more recent studies (Table 1). Despite these differences,

https://doi.org/10.5194/nhess-2023-52
Preprint. Discussion started: 4 April 2023

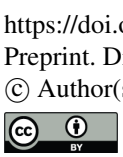

Natural Hazards and Earth System Sciences
Discussions

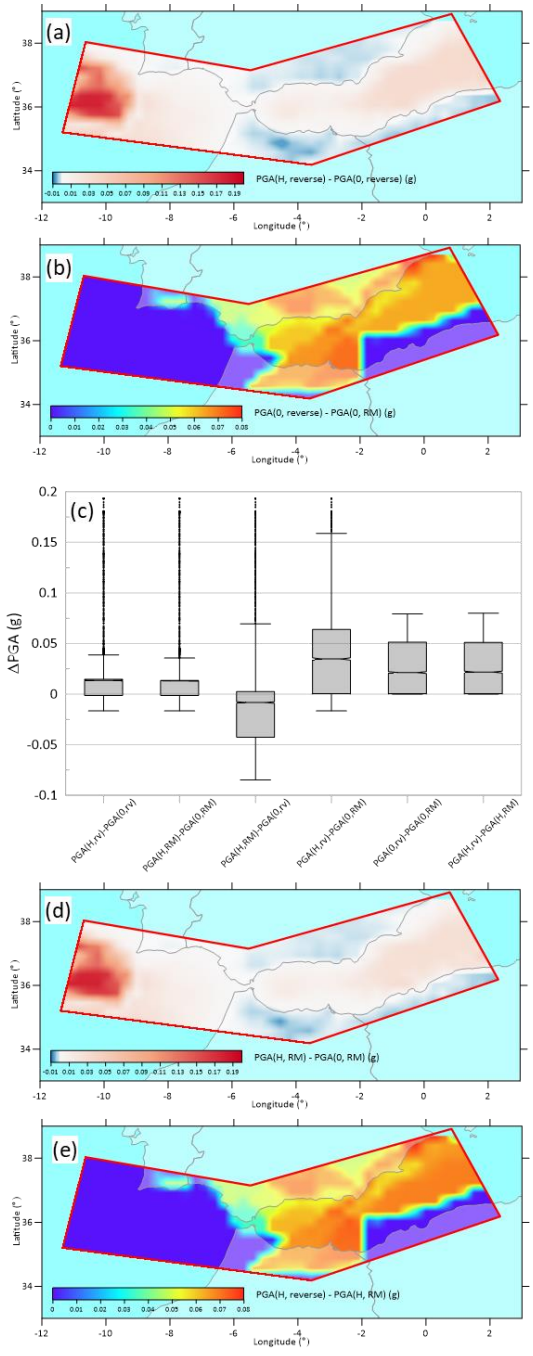

Figure 9. Difference maps between DSHA results in PGA from Figure 8. Substraction: (a) between Figure 7d and a; (b) between Figure 7a and b; (c) Box-Whisker plots fo PGA differences used for Figures 9a,b,d, and e. Center line represents the mean value. Box edges are limited by the quartiles (25% lower and 75% upper percentile). Whiskers are limited by the 1.5 times the inter-quartile range. The notch size factor is 1.7. The sample outliers are represented by dot symbols; (d) difference between Figure 7e and b; (e) difference between Figure 7d and e.

https://doi.org/10.5194/nhess-2023-52
Preprint. Discussion started: 4 April 2023

Natural Hazards and Earth System Sciences Discussions

the spatial correspondence and complete distribution of the values in the region, compared to the partial distributions covered by previous work (Fig. 10) are very similar to that obtained in this work. Although it is not the purpose of this paper to discuss the compatibility, lateral, and comparative continuity of the presented maps, it is possible to appreciate some differences between them. However, the isovalue curves extracted from the case where the DSHA is calculated with the DTM and the source-specific rupture mode (Fig. 7d) plotted on each of the PGA maps obtained by zoned (Fig. 10a, b and d) and nonzoned (Fig. 10c) PSHA probabilistic methods fit both regionally as a whole, and locally in specific areas, to the geometry of the regions. This fit is found in areas with high PGA values: Gorringe, Horseshoe and Coral Patch to the west, Atlas Mountains and Algerian coast to the southeast, and the Betic mountain range from Málaga to Alicante to the north; as well as in the areas with lower values in the Alboran Sea basin to the east and south of the Gulf of Cádiz.

Table 3: Estimation of PGA (g) at bedrock level by DSHA at each control city and according to the test cases considered in this work: DSHA1 result without bathymetric DTM and considering a single reverse rupture mechanism equal for all seismogenic sources; DSHA2 result without bathymetric DTM and considering a source-specific rupture mechanism (Table 1); DSHA3 result with bathymetric DTM (Figure 7a) and considering a reverse rupture mechanism in all seismogenic sources; DSHA4 result with bathymetric DTM and considering a source-specific rupture mechanism (Table 1); DSHA845 84th percentile with bathymetric DTM and considering a source-specific rupture mechanism (Table 1); DSHA986 98th percentile with bathymetric DTM and considering a source-specific rupture mechanism (Table 1); columns 7 to 9 same as 4 to 6, but using the control and all non-control (NS) sources.

Main Region	City	DSHA[1]	DSHA[2]	DSHA[3]	DSHA[4]	$DSHA_{84}$[5]	$DSHA_{98}$[6]	DSHA[7] all NS	$DSHA_{84}$[8] all NS	$DSHA_{98}$[9] all NS
Southern Iberian Peninsula	Cádiz	0.27	0.22	0.27	0.23	0.43	0.82	0.59	0.79	1.26
	Málaga	0.29	0.24	0.29	0.24	0.46	0.87	0.50	0.48	1.08
	Almería	0.32	0.26	0.32	0.27	0.52	1.01	0.61	0.83	1.33
	Huelva	0.3	0.3	0.3	0.3	0.57	1.10	0.58	0.81	1.31
	Granada	0.29	0.22	0.29	0.22	0.41	0.78	0.49	0.64	0.99
	Alicante	0.38	0.31	0.38	0.31	0.59	1.15	0.59	0.81	1.31
North Africa	Tánger	0.22	0.18	0.22	0.18	0.34	0.65	0.47	0.63	0.99
	Melilla	0.39	0.32	0.39	0.32	0.61	1.18	0.56	0.79	1.31
	Orán	0.47	0.47	0.47	0.47	0.90	1.74	0.59	0.92	1.75

https://doi.org/10.5194/nhess-2023-52
Preprint. Discussion started: 4 April 2023

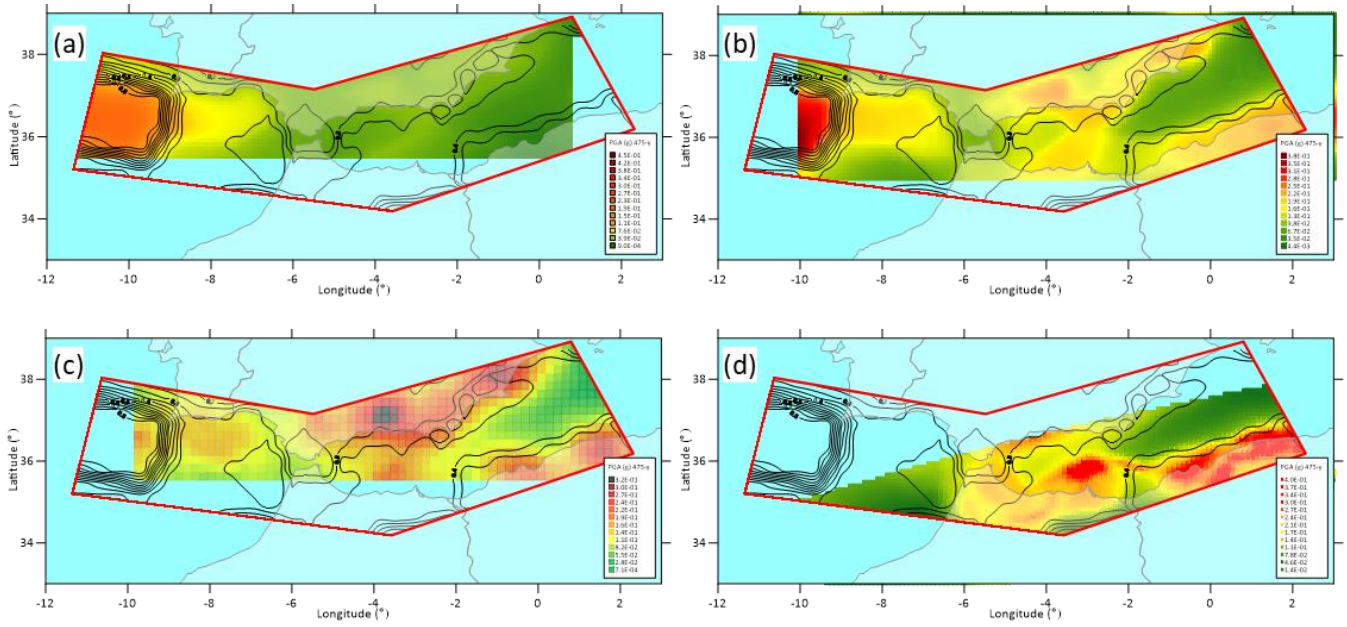

Figure 10. Available PGA (g) maps used in this work for calibrate the results on SHA. South Iberia region PGA map in g from zoned PSHA (a) modified from EHSM13-SHARE Woessner et al. (2015), (b) modified from UPM-IGN (2017), (c) from un-zoned PSHA modified from Crespo et al. (2014), and (d) North Africa region PGA map in g from zoned PSHA modified from Poggi et al. (2020).

5.3 Hazard assessment with exceedance rates and cumulative effect of sources

The results obtained incorporating the uncertainty due to the GMPEs have been carried out considering the DTM in the DSHA calculation, the particular rupture mode of each source, and the random uncertainties σ^{i}_{Y} for each i-th prediction equation, as constants for AKBO10, CAFA08, BOAT08 and BIND11, or evaluated particularly in CHYO14 for the seismic scenario being assessed. The PGA (g) maps obtained for the 16% and 2% exceedance probability values associated with each of them, corresponding to the 84% and 98% percentiles, respectively, of PGA (Fig. 11a and b, respectively) show a geographical distribution of the maximum values over the Atlantic areas of Gorringe, Horseshoe and Coral Patch, and off the Algerian coast in the area of the Mediterranean Alboran basin in both cases of exceedance rates, corresponding to the areas of highest seismogenic potential. The maximum values (Fig. 11c), reach 2 g (maximum at 2.07 g) exceedable by 16% of the cases, with an interquartile range between 0.34 and 0.69 g, with a mean of 0.60 g (PGA(H,RM,84) or PGA_{84}), and up to 4 g (maximum at 4.26 g) with a mean of 1.17 g in a range between 0.66 and 1.33 g, only exceedable by 2% of the cases (PGA(H,RM,98) or PGA_{98}). Therefore, considering random uncertainties in the estimation of hazard by DSHA results in an increase of 103% and 318% for the probability of exceedance of 16% and 2%, respectively, in the maximum PGAs, with smaller increases for the remaining quartiles: 89% and 267% increases for the first quartile of PGA_{84} and PGA_{98}, respectively, and 92% and 269% for the third quartile of the PGA_{84} and PGA_{98} distributions. The multimodal frequency distribution of all these values (Fig. 11d) preserves the shape as the cumulative distribution functions show, maintaining a

https://doi.org/10.5194/nhess-2023-52
Preprint. Discussion started: 4 April 2023

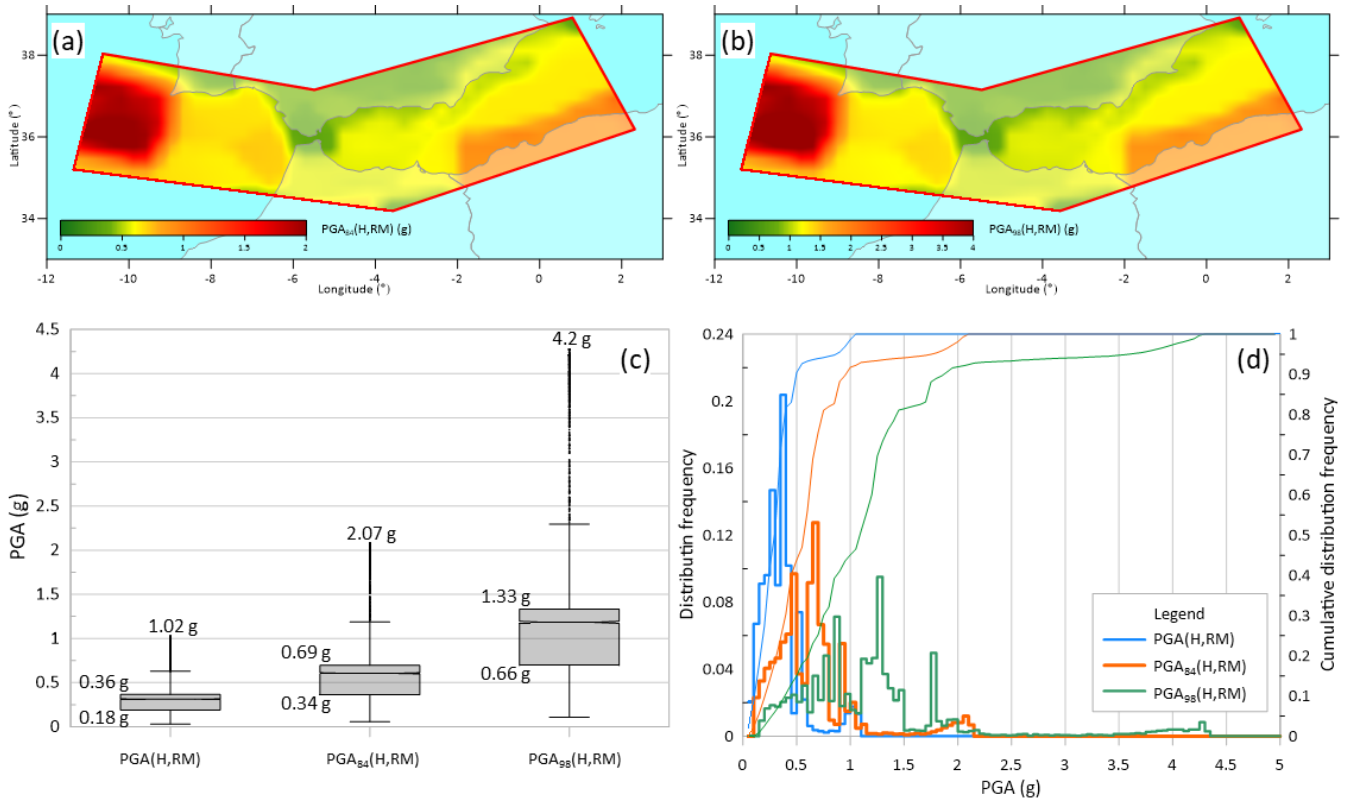

Figure 11. PGA percentile 84 (a) and 98 (b) maps obtained with the DSHA method with DTM (Figure 7a), considering a source-specific average focal mechanism (Table 1) and random uncertainty for each GMPE. (c) Box-Whisker plots for PGA values in Figures (a), (b) and Figure 8d (for comparison). Center line represents the mean value. Box edges are limited by the quartiles (numbers indicated 25% lower and 75% upper percentile). Whiskers are limited by the 1.5 times the inter-quartile range. The notch size factor is 1.7. The sample outliers are represented by dot symbols. (d) Histograms, as distribution of relative frequencies, and experimental cumulative distribution functions for PGA values in Figures (a), (b) and Figure 8d (for comparison).

The regional behaviour shown in the previous results over the studied area is particularly reproduced over the control cities (Fig. 12) in the strong motion they receive, for the control earthquake of each seismogenic source, as a function of distance. In fact, compared to the average values of the PGA marked with blue symbols, the values of the PGA_{84} (yellow dots) increase in the order of 100% and those of the PGA_{98} (red dots) up to 300% approximately and in the same way for all the sources individually, both if the seismic scenario received by the city site is important and if the strong motion is low.

https://doi.org/10.5194/nhess-2023-52
Preprint. Discussion started: 4 April 2023

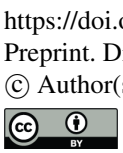

Natural Hazards and Earth System Sciences
Discussions

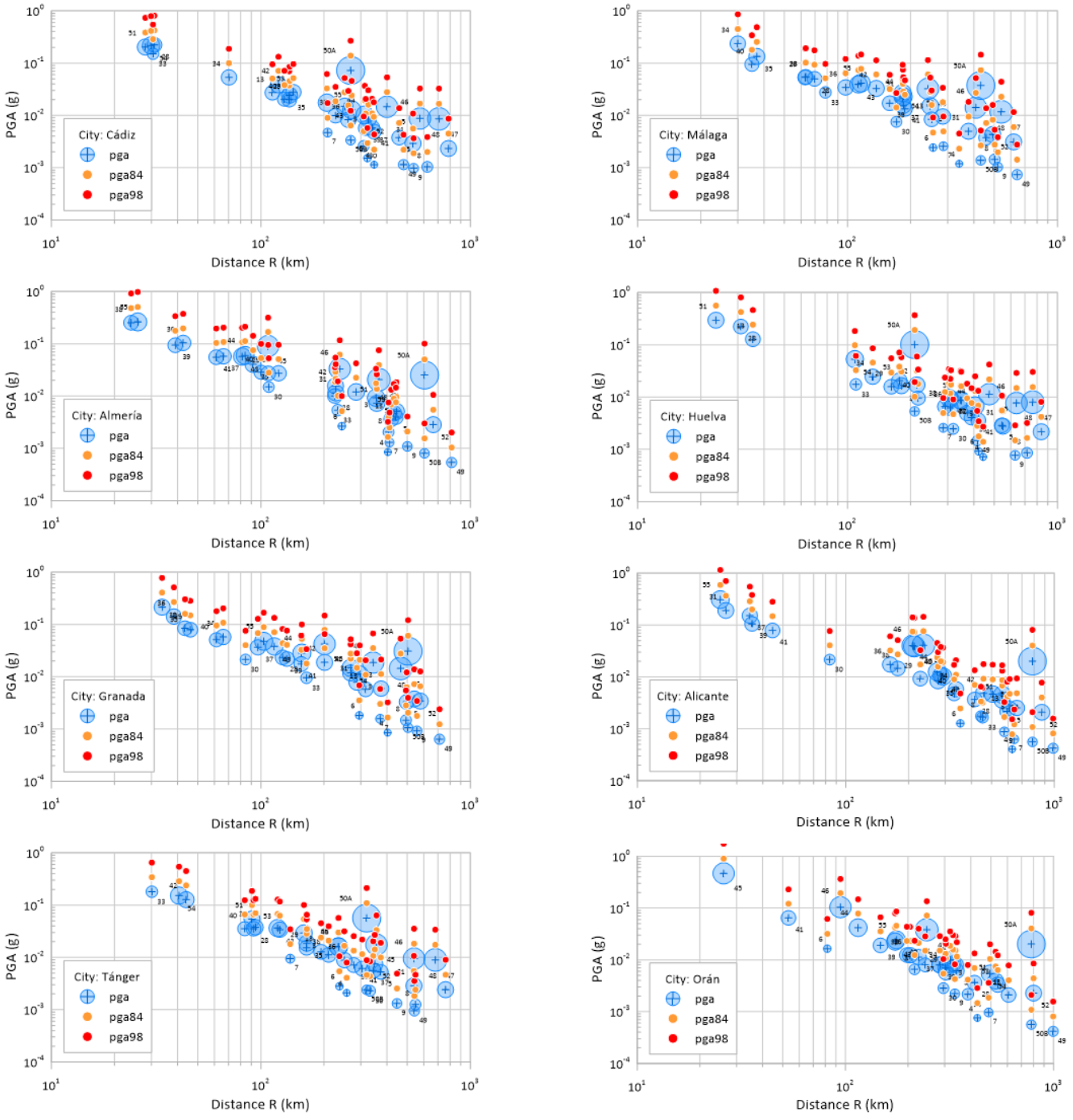

880

Figure 12. Effect of strong seismic motion in each of the control cities triggered from each seismic source, according to its MCE and distance from it, for each of the percentiles (50th median, 84th and 98th) of random uncertainty in the composition of GMPEs. The PGA (in g) has been evaluated considering the type of rupture at each source, and the distance taking into account the DTM, and the depth of each source.

https://doi.org/10.5194/nhess-2023-52
Preprint. Discussion started: 4 April 2023


Natural Hazards and Earth System Sciences Discussions

Specifically, the values of PGA_{84} (Table 3, column $DSHA_{84}$[5]) in the cities of Almeria and Orán do not exceed an increase of 92%, while in Cádiz and Granada they only increase by 86%. As for the PGA_{98} values (Table 3, column $DSHA_{98}$[6]), the maximum increases reach 270% in Almeráa and Orán, with the lowest increases being 255% in Cádiz and Granada. However, the way in which this movement is received is not the same for all cities. The distribution of the PGA in the distance is homogeneously distributed in cities such as Málaga, Granada, and Orán, and there are less homogeneous distributions forming weakly differentiated aggregates such as in Cádiz or Alicante, and two clearly distinguishable source aggregates such as in Almeria, Huelva, or Tánger.

Using the same input data as for the 0.5, 0.16 and 0.02 exceedance probabilities maps shown in Fig. 7 and 11 and calculated with the DSHA method above, using the seismogenic source that produces the maximum ground motion or control earthquake at the site, the hazard calculation for the different percentiles, the DSHA has been calculated using all sources, including those that do not control (Fig. 13). In other words, for this new map, equation (7) has been solved for each point, considering the effect of the distribution of the rest of the seismic scenarios that each source originates, as a non-homogeneous distribution of the seismic scenarios, as found in the control cities (Fig. 12), and the random uncertainty produced by the GMPEs. After considering the joint effect of the 35 sources to create the maps for the mean PGA (PGA(H,RM,NS) in Fig. 13a) and the 84th and 98th percentiles (PGA_{84}(H,RM,NS) and PGA_{98}(H,RM,NS) in Fig. 13b and 13c), a substantial increase in seismic hazard is observed at all points in the study region. This increase is especially higher in areas close to confluences, contact zones, or common sides between seismic zones, being less relevant as the excess probability decreases, becoming barely perceptible in the case of probability 0.02 (Fig. 13c). This geographical distribution reflects the joint nature of the effect of the sources when evaluating the DSHA, increasing by more than 155% in cities such as Cádiz (by 156%) or Tánger (by 161%) for their average GMPEs of 0.59 g and 0.47 g, respectively, when considering all sources in addition to the control source (Table 3, column DSHA[7] all NS), compared to their average PGA values considering only the control source in the calculation of the DSHA with DTM and a particular rupture mechanism (Table 3, column DSHA[4]). The hazard values in these cities can be as high as 1.26 and 0.99 g, 447% and 450%, respectively, when considering probability of exceedance rates of 0.16 and 0.02 over the random uncertainty (Table 3, columns $DSHA_{84}$[8], and $DSHA_{98}$[9] all NS). The cities with the smallest increase are Melilla and Orán, with an increase of 75% and 25% compared to their average comparison PGA values (Table 3, column DSHA[4]). For the rest of the cities, the effect of the increase in their hazard values when including all random sources (Table 3, columns DSHA7, $DSHA_{84}$[8], and $DSHA_{98}$[9] all NS) against the comparison PGA averages is between the extreme values indicated, according to the evaluated AMP percentile.

An overview of the statistical quartile of the increase in the distribution of the PGA-mapped values distributed over the study area can be seen in the Box-Whisker graph (Fig. 13d) and the cumulative frequency distributions for the mean and the 84th and 98th percentiles (Fig. 11e), compared to the corresponding ones obtained in the DSHA study evaluated with the control source alone (Fig. 11c and 11d). The entire distribution of PGA values has increased. Although the maximum values

https://doi.org/10.5194/nhess-2023-52
Preprint. Discussion started: 4 April 2023

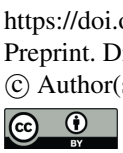

Natural Hazards and Earth System Sciences
Discussions

are almost similar, most of the distribution, comprised of the second and third quartiles, rises in the diagram (Fig. 13d) with the interquartile range of the values remaining almost the same without considering all sources. Even the minima of the PGA for the three evaluated percentiles of the PGA have increased, as seen in the small shift to the right of the cumulative frequency distribution curves (Fig. 13e) which is as much as 470%, for example, between PGA(H,RM) with a minimum of 0.03 g and PGA(H,RM,NS) with 0.17 g, although these distribution functions preserve their shape in terms of the small jumps they present, they are slightly shifted towards higher values of the PGA.

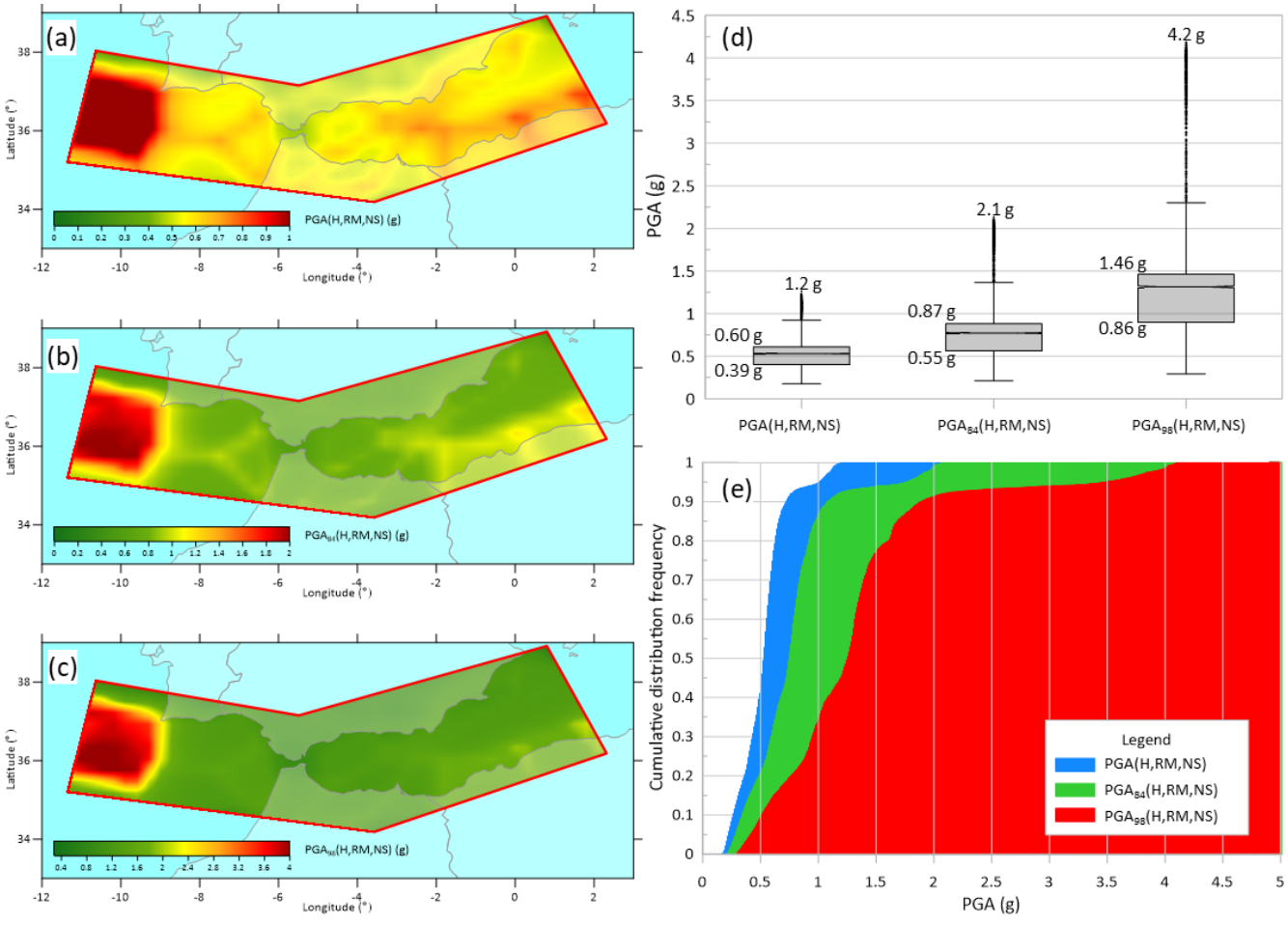

Figure 13. PGA percentile 50 (a), 84 (b) and 98 (c) maps obtained with the DSHA method with DTM (Figure 7a), considering a source-specific average focal mechanism (Table 1), random uncertainty for each GMPE, and cumulative effect on each site of all non-controlling seismogenic sources. (d) Box-Whisker plots for PGA values in (a), (b) and (c). Center line represents the mean value. Box edges are limited by the quartiles (numbers indicated 25% lower and 75% upper percentile). Whiskers are limited by the 1.5 times the inter-quartile range. The notch size factor is 1.7. The sample outliers are represented by dot symbols. (d) Experimental cumulative distribution functions for PGA values in (a), (b) and (c).

https://doi.org/10.5194/nhess-2023-52
Preprint. Discussion started: 4 April 2023

6. Discussion

With the integration of the relevant zonation models used in this work, a catalogue of 35 seismogenic sources has been created, compiling their essential seismic parameters: depth, MCE and rupture mode, to analyse the three-dimensional SHA, using the DTM of the area, according to the deterministic method and with the aim of studying the sensitivity of the results to the variation of these parameters. Most seismic hazard analysis studies worldwide are carried out on emerged lands (e.g., Giardini et al., 2014; IGN-UPM, 2017; Mourabit et al., 2014; Pailoplee et al., 2009; Poggi et al., 2020; Vilanova and Fonseca, 2007; Woessner et al., 2015), so not considering the DTM in the calculation is on the side of the most conservative safety. However, in the case of underwater areas, the distance to the sources is a factor that, if treated in the same way as for land above sea level, leads to incorrect results, underestimating the intensity of the seismic movement, this defect being more noticeable in the deeper areas. On the other hand, the use of the characterisation of the predominant rupture mode in each seismogenic zone is preferable to using a homogeneous global style for the whole study area to avoid uniformising the deformation-tectonic stress regime over the entire area. As the rupture regime of each source enters the calculation process through each GMPE in the structure of the logic tree, therefore only those GMPEs that consider a different formulation for each regime (Douglas, 2001, 2020) will be affected. As in the logic tree used in this work only the CAFA08 GMPE is independent of the rupture mode, the results obtained are affected, to a greater or lesser extent, especially in the areas of low moderate seismic activity in the Alboran basin, since its predominant mode is rupture, and in the emerged territories of the south of the Iberian Peninsula where the mode is mostly normal. The differences between using or not using a DTM in the calculation of the DSHA are more important the higher the seismic activity, although the contribution to these differences is practically negligible for sources that are more than 100 km away. It is precisely in these areas that the differences between considering the local seismogenic peculiarities specified in the constructed catalogue and the DTM are greatest.

Regarding the PGA map obtained with the DTM and each source with its rupture mode, for an exceedance probability rate of 0.5 (50th percentile of the PGA) the qualitative differences, as they are not quantitatively comparable results with other maps that partially provide the offshore PGA distribution, are distinguishable local differences between one and the other. While the DSHA evaluates the worst-case scenario and presents the values of ground motion related to the worst-case scenario, the PSHA allows determining the exceedance rates of the specified ground motion at a desired time. Therefore, a direct comparison between DSHA and PSHA results does not make sense, but the regional trend over the large zones of maximum values (Gorringe, Planicia Horseshoe, Coral Patch areas, in the Atlantic sector, and Arzew Faults Algerian zone, in the Mediterranean), minimum and intermediate PGA values is similar to that obtained in this work with DSHA despite the maps obtained with PSHA methods (UPM-IGN, 2017 and Poggi et al., 2020), with a different zonation (Woessner et al., 2015), or with a nonzoned method (Crespo et al., 2014).

DSHA, unlike other SHA methods, is not affected by the uncertainty of the seismic parameters, as handled by the

https://doi.org/10.5194/nhess-2023-52
Preprint. Discussion started: 4 April 2023

method, which can be very relevant in areas where a complete comprehensive fault-specific catalogue of faults and their activity is not available for a robust estimation. Although, as Reiter (1990) points out, the DSHA does not contemplate the inherent uncertainty in the estimation of seismic risk, since the frequency of occurrence is not explicitly taken into account, i.e., the recurrence interval or frequency and its associated uncertainty are not addressed. A less accurate version, but one that at the same time distributes the uncertainty due to randomness in the attenuation functions over a large region is preferable, even though it provides larger values; these can be used as an upper bound of those that can be achieved, for different exceedance probabilities, such as those applied in this work of 0.16 and 0.02, rather than working with more precise, but less accurate values.

Finally, it should also be emphasised that this study introduces a modified DSHA method incorporating the attenuated effect of all sources in addition to the control source used in the classical DSHA, but does not conclude that the original framework is fundamentally flawed. Once the 35 noncontrol sources are considered, the PGA map indicates a substantial increase in seismic hazard, especially in areas close to the confluence of seismic zones. The joint contribution of the sources to the calculated exceedance probability differs according to the PGA vs. distance pattern at each site. Thus, in the cities used as control points, some cities such as Cádiz and Tánger show larger increases than others such as Melilla or Orán. Consequently, large noncontrollable risks lead to a high estimate (at the same percentile), with extreme probability estimates. The distribution of the PGA over the study area becomes more uniform, with less appreciable changes, as the percentile increases (or the probability of exceedance decreases) although its silhouette in the probability distribution is preserved by extending towards higher PGA values.

Taking this into account, the choice of a seismic hazard alternative should be closely related to the intended applications. For industrial facilities of important socioeconomic position, where failure consequences are unsustainable, it is suggested to use the new DSHA to include the seismic hazard from noncontrolling sources in order to ensure that the design is as safe as possible; conversely, the conventional DSHA might be suitable for noncritical building or structure designs. Similarly, for the study of landslide-triggering hazard that can cause a tsunami, it is also relevant to include all sources, preferably at the point event (Collico et al., 2020) and to use the entire PGA map to apply slope stability methods based on different models (Wang et al., 2021) since underestimating the amplitude of the tsunamigenic source can have catastrophic consequences on the coastline it reaches, so in order not to underestimate the effects and thus the mitigation measures, it is advisable to have an upper bound on the uncertainties (Zengaffinen-Morris et al., 2022). However, the decision for the SHA method is not because the selected method is more scientific than another, since earthquakes are random and unpredictable and hazard estimates are not verifiable (Musson, 2012b, a; Wang, 2012). The PSHA, for example, is questioned for its imperfect algorithm and unrealistic estimates (Castaños and Lomnitz, 2002; Klügel, 2007). Moreover, its use of a logic tree analysis to consolidate so-called epistemic uncertainty is considered unscientific (Krinitzsky 2003). Mualchin (2005) considered that no seismic hazard analysis is perfect given our limited understanding of the random process of earthquakes.

https://doi.org/10.5194/nhess-2023-52
Preprint. Discussion started: 4 April 2023

7. Conclusions

The prediction of tsunamigenic sources, both seismic and co-seismic submarine landslides, has become a controversial topic of current scientific and technical interest in the context of recent tsunamis. Under these circumstances, seismic hazard analysis in marine areas should become a best practice for assessing coastal tsunami hazard in order to develop coastal inundation prevention and mitigation programmes. However, even the analysis of seismic hazard in underwater areas is subject to debate due not only to the fact that it is usually not shown on national seismic hazard maps because it is of no interest in the absence of structures resting on the ground shaken by the earthquake, but also because of its possible shortcomings using standard methodologies. Among these, DSHA also faces this problem. The use of the 50th percentile motion may be insufficient when field evidence indicates that actual seismic motions can sometimes be two or even three standard deviations above the central value, which could lead to seafloor dislocation or a landslide large enough to generate a tsunami.

The results have shown that if the influence of several relevant sources is not fully addressed in the DSHA analysis, it may result in an inadequate SHA, especially when there are numerous sources around the analysed site. Therefore, this study introduces a DSHA that considers non-controlling seismic sources and non-controlling seismic sources using extreme likelihood theory. With this method applied to a submarine region and considering the DTM of bathymetries, a hazard map is presented for the Ibero-Maghreb-Algerian marine area, comprised between the western edge of the Gulf of Cádiz and the eastern Mediterranean boundary of the Alboran basin, considering 35 seismogenic sources with their seismic parameters, rupture mode and depth. Compared to the original DHSA, a substantial increase in the intensity of seismic motion is observed, especially at locations close to the confluence of seismic source zones. This acceleration increases as a lower random uncertainty exceedance probability is used. Therefore, this method based on DSHA is suggested to be applied in submarine areas, to evaluate the genesis of tsunamis by strong motions triggering possible large tsunamigenic landslides, making the hazard assessment as safe as possible with the seismic risks provided by each of the seismic sources.

Code availability

Excel-based Visual Basic script used in this research can be obtained from the corresponding author upon reasonable request.

Data availability

This work used only published or public domain datasets: IGN-UPM (2017, https://doi.org/10.7419/162.05.2017) for Southern Iberian Peninsula; Poggi et al. (2020, https://doi.org/10.1007/s10518-020-00820-4) for North Africa.

https://doi.org/10.5194/nhess-2023-52
Preprint. Discussion started: 4 April 2023

Author contributions

AJRB, CPB and MLLI: Investigation. AJRB: literature review. AJRB, CPB and MLLI: conceptualization. AJRB and CPB: methodology. CPB: software. AJRB and CPB: formal analysis. AJRB: writing (original draft). AJRB, CPB and MLLI: writing (review and editing). CPB and MLLI: supervision. MLLI: validation.

Competing interests

The authors have no relevant competitive or financial interests to disclose.

Acknowledgements

The authors would like to express their gratitude to the anonymous reviewers whose suggestions helped improve and clarify this manuscript. The Open Access publishing for this study has been covered thanks to a CSIC agreement with Copernicus Publications. Thanks to the EMODnet Bathymetry Consortium (2020), EMODnet Digital Bathymetry (DTM). (https://doi.org/10.12770/bb6a87dd-e579-4036-abe1-e649cea9881a) to allow the download and use of the current EMODnet DTM version of December 2020, which has a resolution of 1/16 * 1/16 arc minutes.

References

AEIS-IGN: Seminario sobre criterios sísmicos para centrales nucleares y obras públicas: Madrid, 29-30 de marzo de 1978, Asoc. Esp. Ing. Sísmica AEIS Inst. Geográfico Nac. IGN, 1979.

Akkar, S. and Bommer, J. J.: Empirical Equations for the Prediction of PGA, PGV, and Spectral Accelerations in Europe, the Mediterranean Region, and the Middle East, Seismol. Res. Lett., 81, 195–206, https://doi.org/10.1785/gssrl.81.2.195, 2010.

Ang, A. H. and Tang, W. H.: Probability Concepts in Engineering Planning: Emphasis on Applications to Civil and Environmental Engineering, John Wiley and Sons, 2007.

Arenillas, M., C, S., and A, S.: CRITERIA TO DETERMINE SEISMIC RISK ON SITES: APPLICATION TO SPANISH DAMS, 1982.

Atkinson, G. M., Bommer, J. J., and Abrahamson, N. A.: Alternative Approaches to Modeling Epistemic Uncertainty in Ground Motions in Probabilistic Seismic-Hazard Analysis, Seismol. Res. Lett., 85, 1141–1144, https://doi.org/10.1785/0220140120, 2014.

Atkinson, K.: An Introduction to Numerical Analysis, John Wiley & Sons, 726 pp., 1991.

Benito, B. and Jiménez, E.: Peligrosidad sísmica, Física Tierra, 11, 13–47, 1999.

Ben-Zion, Y., Lee, W. H. K., Kanamori, H., Jennings, P. C., and Kisslinger, C.: Key formulas in earthquake seismology, Int. Handb. Earthq. Eng. Seismol., 81, 1857–1875, 2003.

Beven, K. J., Almeida, S., Aspinall, W. P., Bates, P. D., Blazkova, S., Borgomeo, E., Freer, J., Goda, K., Hall, J. W., Phillips, J. C., Simpson, M., Smith, P. J., Stephenson, D. B., Wagener, T., Watson, M., and Wilkins, K. L.: Epistemic uncertainties and natural hazard risk assessment – Part 1: A review of different natural hazard areas, Nat. Hazards Earth Syst. Sci., 18, 2741–2768, https://doi.org/10.5194/nhess-18-2741-2018, 2018.

Bezzeghoud, M., Ayadi, A., Caldeira, B., Fontiela, J., and Borges, J. F.: Los mayores sismos en Argelia en la época moderna: las fallas de El Asnam y Zemmouri-Boumerdès, Fis. Tierra, 29, 183, 2017.

Bindi, D., Pacor, F., Luzi, L., Puglia, R., Massa, M., Ameri, G., and Paolucci, R.: Ground motion prediction equations derived from the Italian strong motion database, Bull. Earthq. Eng., 9, 1899–1920, https://doi.org/10.1007/s10518-011-9313-z, 2011.

Bommer, J. J.: Deterministic vs. probabilistic seismic hazard assessment: an exaggerated and obstructive dichotomy, J. Earthq. Eng., 06, 43–73, https://doi.org/10.1142/S1363246902000644, 2002.

Bommer, J. J.: Uncertainty about the uncertainty in seismic hazard analysis, Eng. Geol., 70, 165–168, https://doi.org/10.1016/S0013-7952(02)00278-8, 2003.

Bommer, J. J. and Scherbaum, F.: The Use and Misuse of Logic Trees in Probabilistic Seismic Hazard Analysis, Earthq. Spectra, 24, 997–1009, https://doi.org/10.1193/1.2977755, 2008.

Bommer, J. J., Scherbaum, F., Bungum, H., Cotton, F., Sabetta, F., and Abrahamson, N. A.: On the Use of Logic Trees for Ground-Motion Prediction Equations in Seismic-Hazard Analysis, Bull. Seismol. Soc. Am., 95, 377–389, https://doi.org/10.1785/0120040073, 2005.

Bommer, J. J., Douglas, J., Scherbaum, F., Cotton, F., Bungum, H., and Fäh, D.: On the Selection of Ground-Motion Prediction Equations for Seismic Hazard Analysis, Seismol. Res. Lett., 81, 783–793, https://doi.org/10.1785/gssrl.81.5.783, 2010.

Bommer, J. J., Akkar, S., and Drouet, S.: Extending ground-motion prediction equations for spectral accelerations to higher response frequencies, Bull. Earthq. Eng., 10, 379–399, https://doi.org/10.1007/s10518-011-9304-0, 2012.

Boore, D. M. and Atkinson, G. M.: Ground-Motion Prediction Equations for the Average Horizontal Component of PGA, PGV, and 5%-Damped PSA at Spectral Periods between 0.01 s and 10.0 s, Earthq. Spectra, 24, 99–138, https://doi.org/10.1193/1.2830434, 2008.

Budnitz, R. J., Apostolakis, G., and Boore, D. M.: Recommendations for probabilistic seismic hazard analysis: Guidance on uncertainty and use of experts, US Nuclear Regulatory Commission (NRC), Washington, DC (United States). Div. of Engineering Technology; Lawrence Livermore National Lab. (LLNL), Livermore, CA (United States); Electric Power Research Inst. (EPRI), Palo Alto, CA (United States); US Department of Energy (USDOE), Washington DC (United States), https://doi.org/10.2172/479072, 1997.

Buforn, E. and Udías, A.: Sismicidad y mecanismo focal de los terremotos de la región Cabo de San Vicente-Argelia, Rev. Soc. Geológica Esp., 20, 301–310, 2007.

Buforn, E., Sanz de Galdeano, C., and Udías, A.: Seismotectonics of the Ibero-Maghrebian region, Tectonophysics, 248, 247–261, https://doi.org/10.1016/0040-1951(94)00276-F, 1995.

Buforn, E., Bezzeghoud, M., UdÍas, A., and Pro, C.: Seismic Sources on the Iberia-African Plate Boundary and their Tectonic Implications, Pure Appl. Geophys., 161, 623–646, https://doi.org/10.1007/s00024-003-2466-1, 2004.

https://doi.org/10.5194/nhess-2023-52
Preprint. Discussion started: 4 April 2023

Burden, R. L., Faires, J. D., and Burden, A. M.: Numerical Analysis, Cengage Learning, 918 pp., 2015.

Campbell, K.: Overview of Seismic hazard Approaches with Emphasis on the Management of Uncertainties.“, in: 2nd ICTP Workshop on Earthquake Engineering for Nuclear Facilities: Uncertainties in Seismic Hazard”, Trieste, Italy, 14–25, 2005.

Candia, G., Macedo, J., Jaimes, M. A., and Magna-Verdugo, C.: A New State-of-the-Art Platform for Probabilistic and Deterministic Seismic Hazard Assessment, Seismol. Res. Lett., 90, 2262–2275, https://doi.org/10.1785/0220190025, 2019.

Carvalho, A. M. and Malfeito, N.: Mapas de perigosidade sísmica para Portugal Continental: Uma análise crítica - Parte I – Períodos de recorrência de sismos, 2018.

Castaños, H. and Lomnitz, C.: PSHA: is it science?, Eng. Geol., 66, 315–317, https://doi.org/10.1016/S0013-7952(02)00039-X, 2002.

Cauzzi, C. and Faccioli, E.: Broadband (0.05 to 20 s) prediction of displacement response spectra based on worldwide digital records, J. Seismol., 12, 453–475, https://doi.org/10.1007/s10950-008-9098-y, 2008.

CEN: Design of structures for earthquake resistance—part 1: General rules, seismic actions and rules for buildings, Eur. Comm. Stand. CEN Bruss., BS EN 1998–1:2004, 2004.

Chen, Y.-S., Weatherill, G., Pagani, M., and Cotton, F.: A transparent and data-driven global tectonic regionalization model for seismic hazard assessment, Geophys. J. Int., 213, 1263–1280, https://doi.org/10.1093/gji/ggy005, 2018.

Cheng, C.-T., Chiou, S.-J., Lee, C.-T., and Tsai, Y.-B.: Study on probabilistic seismic hazard maps of Taiwan after Chi-Chi earthquake, J. Geoengin., 2, 19–28, https://doi.org/10.6310/jog.2007.2(1).3, 2007.

Chiou, B. S.-J. and Youngs, R. R.: Update of the Chiou and Youngs NGA Model for the Average Horizontal Component of Peak Ground Motion and Response Spectra, Earthq. Spectra, 30, 1117–1153, https://doi.org/10.1193/072813EQS219M, 2014.

Chiou, B.-J. and Youngs, R. R.: An NGA Model for the Average Horizontal Component of Peak Ground Motion and Response Spectra, Earthq. Spectra, 24, 173–215, https://doi.org/10.1193/1.2894832, 2008.

Coles, S.: An Introduction to Statistical Modeling of Extreme Values, Springer, London, https://doi.org/10.1007/978-1-4471-3675-0, 2001.

Collico, S., Arroyo, M., Urgeles, R., Gràcia, E., Devincenzi, M., and Peréz, N.: Probabilistic mapping of earthquake-induced submarine landslide susceptibility in the South-West Iberian margin, Mar. Geol., 429, 106296, https://doi.org/10.1016/j.margeo.2020.106296, 2020.

Coppersmith, K. J. and Youngs, R. R.: Capturing uncertainty in probabilistic seismic hazard assessments within intraplate tectonic environments, in: Proceedings of the Third US national conference on earthquake engineering, 301–312, 1986.

Corbi, F., Sandri, L., Bedford, J., Funiciello, F., Brizzi, S., Rosenau, M., and Lallemand, S.: Machine Learning Can Predict the Timing and Size of Analog Earthquakes, Geophys. Res. Lett., 46, 1303–1311, https://doi.org/10.1029/2018GL081251, 2019.

Cornell, C. A.: Engineering seismic risk analysis, Bull. Seismol. Soc. Am., 58, 1583–1606, https://doi.org/10.1785/BSSA0580051583, 1968.

Cornell, C. A., Howells, D. A., Haigh, I. P., and Taylor, C.: Probabilistic analysis of damage to structures under seismic loads, Dyn. Waves Civ. Eng., 473–488, 1971.

Cotton, F., Scherbaum, F., Bommer, J. J., and Bungum, H.: Criteria for Selecting and Adjusting Ground-Motion Models for Specific Target Regions: Application to Central Europe and Rock Sites, J. Seismol., 10, 137–156, https://doi.org/10.1007/s10950-005-9006-7, 2006.

Crespo, M. J., Martínez, F., and Martí, J.: Seismic hazard of the Iberian Peninsula: evaluation with kernel functions, Nat. Hazards Earth Syst. Sci., 14, 1309–1323, https://doi.org/10.5194/nhess-14-1309-2014, 2014.

Custódio, S., Lima, V., Vales, D., Cesca, S., and Carrilho, F.: Imaging active faulting in a region of distributed deformation from the joint clustering of focal mechanisms and hypocentres: Application to the Azores–western Mediterranean region, Tectonophysics, 676, 70–89, https://doi.org/10.1016/j.tecto.2016.03.013, 2016.

Delavaud, E., Cotton, F., Akkar, S., Scherbaum, F., Danciu, L., Beauval, C., Drouet, S., Douglas, J., Basili, R., Sandikkaya, M. A., Segou, M., Faccioli, E., and Theodoulidis, N.: Toward a ground-motion logic tree for probabilistic seismic hazard assessment in Europe, J. Seismol., 16, 451–473, https://doi.org/10.1007/s10950-012-9281-z, 2012.

Douglas, J.: A comprehensive worldwide summary of strong-motion attenuation relationships for peak ground acceleration and spectral ordinates (1969 to 2000), Imperial College of Science, Technology and Medicine, Civil Engineering …, 2001.

Douglas, J.: Ground motion prediction equations 1964–2020, Dept Civ. Env. Eng Univ Strathclyde Glas. UK, 670, 2020.

El Alami, S. O., Tadili, B. A., Cherkaoui, T. E., Medina, F., Ramdani, M., Brahim, L. A., and Harnafi, M.: The Al Hoceima earthquake of May 26, 1994 and its aftershocks: a seismotectonic study, 1998.

EPRI: Seismic hazard methodology for the central and eastern United States, Seysmicity Own. Group Electr. Power Res. Inst. EPRI, P101-38-45–46, 2256–14, Report NP-472, 1987.

Epstein, B. and Lomnitz, C.: A Model for the Occurrence of Large Earthquakes, Nature, 211, 954–956, https://doi.org/10.1038/211954b0, 1966.

Estrada, F., Galindo-Zaldívar, J., Vázquez, J. T., Ercilla, G., D'Acremont, E., Alonso, B., and Gorini, C.: Tectonic indentation in the central Alboran Sea (westernmost Mediterranean), Terra Nova, 30, 24–33, https://doi.org/10.1111/ter.12304, 2018.

Fonseca, J. F. B. D.: A Reassessment of the Magnitude of the 1755 Lisbon Earthquake, Bull. Seismol. Soc. Am., 110, 1–17, https://doi.org/10.1785/0120190198, 2020.

Galindo-Zaldívar, J., Chalouan, A., Azzouz, O., Sanz de Galdeano, C., Anahnah, F., Ameza, L., Ruano, P., Pedrera, A., Ruiz-Constán, A., Marín-Lechado, C., Benmakhlouf, M., López-Garrido, A. C., Ahmamou, M., Saji, R., Roldán-García, F. J., Akil, M., and Chabli, A.: Are the seismological and geological observations of the Al Hoceima (Morocco, Rif) 2004 earthquake (M=6.3) contradictory?, Tectonophysics, 475, 59–67, https://doi.org/10.1016/j.tecto.2008.11.018, 2009.

Galindo-Zaldivar, J., Ercilla, G., Estrada, F., Catalán, M., d'Acremont, E., Azzouz, O., Casas, D., Chourak, M., Vazquez, J. T., Chalouan, A., Sanz de Galdeano, C., Benmakhlouf, M., Gorini, C., Alonso, B., Palomino, D., Rengel, J. A., and Gil, A. J.: Imaging the Growth of Recent Faults: The Case of 2016–2017 Seismic Sequence Sea Bottom Deformation in the Alboran Sea (Western Mediterranean), Tectonics, 37, 2513–2530, https://doi.org/10.1029/2017TC004941, 2018.

Galindo-Zaldivar, J., Gil, A. J., Tendero-Salmerón, V., Borque, M. J., Ercilla, G., González-Castillo, L., Sánchez-Alzola, A., Lacy, M. C., Estrada, F., Avilés, M., Alfaro, P., Madarieta-Txurruka, A., and Chacón, F.: The Campo de Dalias GNSS Network Unveils the Interaction between Roll-Back and Indentation Tectonics in the Gibraltar Arc, Sensors, 22, 2128, https://doi.org/10.3390/s22062128, 2022.

García Mayordomo, J.: Creación de un modelo de zonas sismogénicas para el cálculo del Mapa de Peligrosidad Sísmica de España, CSIC - Instituto Geológico y Minero de España (IGME), 2015.

García-Fernández, M., Vaccari, F., Jiménez, M.-J., Magrin, A., Romanelli, F., and Panza, G. F.: Chapter 24 - Regional application of the NDSHA approach for continental seismogenic sources in the Iberian Peninsula, in: Earthquakes and Sustainable Infrastructure, edited by: Panza, G. F., Kossobokov, V. G., Laor, E., and De Vivo, B., Elsevier, 491–514, https://doi.org/10.1016/B978-0-12-823503-4.00006-3, 2022.

GEBCO Compilation Group 2022: The GEBCO_2022 Grid - a continuous terrain model of the global oceans and land, NERC EDS Br. Oceanogr. Data Cent. NOC, https://doi.org/10.5285/e0f0bb80-ab44-2739-e053-6c86abc0289c, 2022.

Geller, R. J., Jackson, D. D., Kagan, Y. Y., and Mulargia, F.: Earthquakes Cannot Be Predicted, Science, 275, 1616–1616, https://doi.org/10.1126/science.275.5306.1616, 1997.

Giardini, D., Woessner, J., Danciu, L., Crowley, H., Cotton, F., Grünthal, G., Pinho, R., Valensise, G., Akkar, S., and Arvidsson, R.: Seismic hazard harmonization in Europe (SHARE): online data resource, Swiss Seism Serv ETH Zurich Zurich Switz, 10, 2013.

Giardini, D., Wössner, J., and Danciu, L.: Mapping Europe's Seismic Hazard, Eos Trans. Am. Geophys. Union, 95, 261–262, https://doi.org/10.1002/2014EO290001, 2014.

Goded, T., Buforn, E., and Muñoz, D.: The 1494 and 1680 Málaga (Southern Spain) Earthquakes, Seismol. Res. Lett., 79, 707–715, https://doi.org/10.1785/gssrl.79.5.707, 2008.

Gómez de la Peña, L., Gràcia, E., Maesano, F. E., Basili, R., Kopp, H., Sánchez-Serra, C., Scala, A., Romano, F., Volpe, M., Piatanesi, A., and R. Ranero, C.: A first appraisal of the seismogenic and tsunamigenic potential of the largest fault systems in the westernmost Mediterranean, Mar. Geol., 445, 106749, https://doi.org/10.1016/j.margeo.2022.106749, 2022.

Gonzalez-Castillo, L., Galindo-Zaldivar, J., de Lacy, M. C., Borque, M. J., Martinez-Moreno, F. J., García-Armenteros, J. A., and Gil, A. J.: Active rollback in the Gibraltar Arc: Evidences from CGPS data in the western Betic Cordillera, Tectonophysics, 663, 310–321, https://doi.org/10.1016/j.tecto.2015.03.010, 2015.

Grasso, S. and Maugeri, M.: The Seismic Microzonation of the City of Catania (Italy) for the Etna Scenario Earthquake (M = 6.2) of 20 February 1818, Earthq. Spectra, 28, 573–594, https://doi.org/10.1193/1.4000013, 2012.

Gumbel, E. J.: Statistics of Extremes, Columbia University Press, https://doi.org/10.7312/gumb92958, 1958.

Hamming, R. W. and Hamming, R. W.: Numerical Methods for Scientists and Engineers, Courier Corporation, 756 pp., 1986.

Hasterok, D., Halpin, J. A., Collins, A. S., Hand, M., Kreemer, C., Gard, M. G., and Glorie, S.: New Maps of Global Geological Provinces and Tectonic Plates, Earth-Sci. Rev., 231, 104069, https://doi.org/10.1016/j.earscirev.2022.104069, 2022.

Hays, W. W., Algermissen, S. T., Espindsa, A. F., Perkins, D. M., and Rinehart, W. A.: Guidelines for developing design earthquake response spectra, Final Report Army Construction Engineering Research Lab, 1975.

Herraiz, M., De Vicente, G., Lindo-Ñaupari, R., Giner, J., Simón, J. L., González-Casado, J. M., Vadillo, O., Rodríguez-Pascua, M. A., Cicuéndez, J. I., Casas, A., Cabañas, L., Rincón, P., Cortés, A. L., Ramírez, M., and Lucini, M.: The recent (upper Miocene to Quaternary) and present tectonic stress distributions in the Iberian Peninsula, Tectonics, 19, 762–786, https://doi.org/10.1029/2000TC900006, 2000.

Huang, D. and Wang, J.-P.: Seismic hazard map around Taiwan through a catalog-based deterministic approach, in: 15th World Conference on Earthquake Engineering, 2012.

IGN: Instituto Geográfico Nacional: Geology and tectonics of Gulf of Cadiz, https://www.ign.es/web/resources/sismologia/tproximos/sismotectonica/pag_sismotectonicas/golfocadiz.html, 2023.

IGN-UPM: Actualización de mapas de peligrosidad sísmica de España 2012, Inst. Geográfico Nac. IGN, 267, https://doi.org/10.7419/162.05.2017, 2017.

Joshi, G. C. and Sharma, M. L.: Uncertainties in the estimation of Mmax, J. Earth Syst. Sci., 117, 671–682, https://doi.org/10.1007/s12040-008-0063-5, 2008.

Kaklamanos, J., Baise, L. G., and Boore, D. M.: Estimating Unknown Input Parameters when Implementing the NGA Ground-Motion Prediction Equations in Engineering Practice, Earthq. Spectra, 27, 1219–1235, https://doi.org/10.1193/1.3650372, 2011.

Kijko, A.: Seismic Hazard, in: Encyclopedia of Solid Earth Geophysics, edited by: Gupta, H. K., Springer International Publishing, Cham, 1–14, https://doi.org/10.1007/978-3-030-10475-7_10-1, 2019.

Kiureghian, A. D. and Ditlevsen, O.: Aleatory or epistemic? Does it matter?, Struct. Saf., 31, 105–112, https://doi.org/10.1016/j.strusafe.2008.06.020, 2009.

Klügel, J.-U.: Error inflation in Probabilistic Seismic Hazard Analysis, Eng. Geol., 90, 186–192, https://doi.org/10.1016/j.enggeo.2007.01.003, 2007.

Knuth, D. E.: The Art of Computer Programming: Volume 3: Sorting and Searching, Addison-Wesley Professional, 804 pp., 1998.

Koulali, A., Ouazar, D., Tahayt, A., King, R. W., Vernant, P., Reilinger, R. E., McClusky, S., Mourabit, T., Davila, J. M., and Amraoui, N.: New GPS constraints on active deformation along the Africa–Iberia plate boundary, Earth Planet. Sci. Lett., 308, 211–217, https://doi.org/10.1016/j.epsl.2011.05.048, 2011.

Kramer, S. L.: Geotechnical Earthquake Engineering, Prentice-Hall Civ. Eng. Eng. Mech. Ser. Prentice Hall Up. Saddle River, 653, 1996.

Krinitzsky, E. L.: Earthquake probability in engineering — Part 1: The use and misuse of expert opinion. The Third Richard H. Jahns Distinguished Lecture in Engineering Geology, Eng. Geol., 33, 257–288, https://doi.org/10.1016/0013-7952(93)90030-G, 1993a.

Krinitzsky, E. L.: Earthquake probability in engineering—Part 2: Earthquake recurrence and limitations of Gutenberg-Richter b-values for the engineering of critical structures: The third Richard H. Jahns distinguished lecture in engineering geology, Eng. Geol., 36, 1–52, https://doi.org/10.1016/0013-7952(93)90017-7, 1993b.

Krinitzsky, E. L.: Deterministic versus probabilistic seismic hazard analysis for critical structures, Eng. Geol., 40, 1–7, https://doi.org/10.1016/0013-7952(95)00031-3, 1995.

Krinitzsky, E. L.: How to obtain earthquake ground motions for engineering design, Eng. Geol., 65, 1–16, https://doi.org/10.1016/S0013-7952(01)00098-9, 2002.

Krinitzsky, E. L.: Comment on J.U. Klügel's "Problems in the application of the SSHAC probability method for assessing earthquake hazards at Swiss nuclear power plants", in Engineering Geology, vol. 78, pp. 285–307, Eng. Geol., 82, 66–68, https://doi.org/10.1016/j.enggeo.2005.09.004, 2005.

Lafosse, M., d'Acremont, E., Rabaute, A., Estrada, F., Jollivet-Castelot, M., Vazquez, J. T., Galindo-Zaldivar, J., Ercilla, G., Alonso, B., Smit, J., Ammar, A., and Gorini, C.: Plio-Quaternary tectonic evolution of the southern margin of the Alboran Basin (Western Mediterranean), Solid Earth, 11, 741–765, https://doi.org/10.5194/se-11-741-2020, 2020.

Leprêtre, R., Frizon de Lamotte, D., Combier, V., Gimeno-Vives, O., Mohn, G., and Eschard, R.: The Tell-Rif orogenic system (Morocco, Algeria, Tunisia) and the structural heritage of the southern Tethys margin, BSGF-Earth Sci. Bull., 189, 10, https://doi.org/10.1051/bsgf/2018009, 2018.

Loi, D. W., Raghunandan, M. E., and Swamy, V.: Revisiting seismic hazard assessment for Peninsular Malaysia using deterministic and probabilistic approaches, Nat. Hazards Earth Syst. Sci., 18, 2387–2408, https://doi.org/10.5194/nhess-18-2387-2018, 2018.

López Casado, C., Molina, S., Giner, J. J., and Delgado, J.: Magnitude-Intensity Relationships in the Ibero-Magrebhian Region, Nat. Hazards, 22, 269–294, https://doi.org/10.1023/A:1008142531071, 2000.

Magrin, A., Peresan, A., Kronrod, T., Vaccari, F., and Panza, G. F.: Neo-deterministic seismic hazard assessment and earthquake occurrence rate, Eng. Geol., 229, 95–109, https://doi.org/10.1016/j.enggeo.2017.09.004, 2017.

Mantovani, E., Albarello, D., and Mucciarelli, M.: Evidence of interconnection between seismic activity in the Iberian Peninsula and North African belts, Phys. Earth Planet. Inter., 54, 116–119, https://doi.org/10.1016/0031-9201(89)90191-X, 1989.

Maramai, A., Brizuela, B., and Graziani, L.: The Euro-Mediterranean Tsunami Catalogue, https://doi.org/10.4401/ag-6437, 2014.

Martín-Dávila, J. and Pazos, A.: Sismicidad del Golfo de Cadiz y zonas adyacentes, Física Tierra ISSN 0214-4557 Nº 15 2003 Pags 189-210, 2003.

Martínez-García, P., Soto, J. I., and Comas, M.: Recent structures in the Alboran Ridge and Yusuf fault zones based on swath bathymetry and sub-bottom profiling: evidence of active tectonics, Geo-Mar. Lett., 31, 19–36, https://doi.org/10.1007/s00367-010-0212-0, 2011.

Mayer, L., Jakobsson, M., Allen, G., Dorschel, B., Falconer, R., Ferrini, V., Lamarche, G., Snaith, H., and Weatherall, P.: The Nippon Foundation—GEBCO Seabed 2030 Project: The Quest to See the World's Oceans Completely Mapped by 2030, Geosciences, 8, 63, https://doi.org/10.3390/geosciences8020063, 2018.

McGuire, R. K.: Seismic hazard and risk analysis, Earthquake Engineering Research Institute, Berkeley, 2004.

McGuire, R. K.: Probabilistic seismic hazard analysis: Early history, Earthq. Eng. Struct. Dyn., 37, 329–338, https://doi.org/10.1002/eqe.765, 2008.

https://doi.org/10.5194/nhess-2023-52
Preprint. Discussion started: 4 April 2023

McGuire, R. K. and Shedlock, K. M.: Statistical uncertainties in seismic hazard evaluations in the United States, Bull. Seismol. Soc. Am., 71, 1287–1308, https://doi.org/10.1785/BSSA0710041287, 1981.

Medialdea, T., Vegas, R., Somoza, L., Vázquez, J. T., Maldonado, A., Díaz-del-Río, V., Maestro, A., Córdoba, D., and Fernández-Puga, M. C.: Structure and evolution of the "Olistostrome" complex of the Gibraltar Arc in the Gulf of Cádiz (eastern Central Atlantic): evidence from two long seismic cross-sections, Mar. Geol., 209, 173–198, https://doi.org/10.1016/j.margeo.2004.05.029, 2004.

Meghraoui, M. and Pondrelli, S.: Active faulting and transpression tectonics along the plate boundary in North Africa, Ann. Geophys., 55, 955, https://doi.org/10.4401/ag-4970, 2012.

Molina Palacios, S.: Sismotectónica y peligrosidad sísmica del área de contacto entre Iberia y África, http://purl.org/dc/dcmitype/Text, Universidad de Granada, 1998.

Montessus de Ballore, F.: La península ibérica sismica y sus colonias, in: Anales de la Sociedad Española de Historia Natural, 175–184, 1894.

Morales, J., Benito, B., and Luján, M.: Expected ground motion in the south-east of Spain due to an earthquake in the epicentral area of the 1910 Adra earthquake, J. Seismol., 7, 175–192, https://doi.org/10.1023/A:1023506015307, 2003.

Moratto, L., Orlecka-Sikora, B., Costa, G., Suhadolc, P., Papaioannou, Ch., and Papazachos, C. B.: A deterministic seismic hazard analysis for shallow earthquakes in Greece, Tectonophysics, 442, 66–82, https://doi.org/10.1016/j.tecto.2007.05.004, 2007.

Mostafa, S. I., Abdelhafiez, H. E., and Abd el-aal, A. el-aziz K.: Deterministic scenarios for seismic hazard assessment in Egypt, J. Afr. Earth Sci., 160, 103655, https://doi.org/10.1016/j.jafrearsci.2019.103655, 2019.

Mourabit, T., Abou Elenean, K. M., Ayadi, A., Benouar, D., Ben Suleman, A., Bezzeghoud, M., Cheddadi, A., Chourak, M., ElGabry, M. N., Harbi, A., Hfaiedh, M., Hussein, H. M., Kacem, J., Ksentini, A., Jabour, N., Magrin, A., Maouche, S., Meghraoui, M., Ousadou, F., Panza, G. F., Peresan, A., Romdhane, N., Vaccari, F., and Zuccolo, E.: Neo-deterministic seismic hazard assessment in North Africa, J. Seismol., 18, 301–318, https://doi.org/10.1007/s10950-013-9375-2, 2014.

Mualchin, L.: Seismic hazard analysis for critical infrastructures in California, Eng. Geol., 79, 177–184, https://doi.org/10.1016/j.enggeo.2005.01.009, 2005.

Munuera, J. M.: Datos básicos para un estudio de sismicidad en el área de la península Ibérica, Mem. Inst. Geográfico Catastral, 32, 1963.

Musson, R. M. W.: Probability in PSHA: Reply to "Comment on 'PSHA Validated by Quasi-Observational Means' by Z. Wang," Seismol. Res. Lett., 83, 717–719, https://doi.org/10.1785/0220120036, 2012a.

Musson, R. M. W.: PSHA Validated by Quasi Observational Means, Seismol. Res. Lett., 83, 130–134, https://doi.org/10.1785/gssrl.83.1.130, 2012b.

National Research Council: Probabilistic seismic hazard analysis, Natl. Acad. Press Washintong DC, 97 pp., 1988.

Negredo, A. M., Bird, P., Sanz de Galdeano, C., and Buforn, E.: Neotectonic modeling of the Ibero-Maghrebian region, J. Geophys. Res. Solid Earth, 107, ETG 10-1-ETG 10-15, https://doi.org/10.1029/2001JB000743, 2002.

https://doi.org/10.5194/nhess-2023-52
Preprint. Discussion started: 4 April 2023

Neres, M., Carafa, M. M. C., Fernandes, R. M. S., Matias, L., Duarte, J. C., Barba, S., and Terrinha, P.: Lithospheric deformation in the Africa-Iberia plate boundary: Improved neotectonic modeling testing a basal-driven Alboran plate, J. Geophys. Res. Solid Earth, 121, 6566–6596, https://doi.org/10.1002/2016JB013012, 2016.

Nocquet, J.-M.: Present-day kinematics of the Mediterranean: A comprehensive overview of GPS results, Tectonophysics, 579, 220–242, https://doi.org/10.1016/j.tecto.2012.03.037, 2012.

NRC: Reactor site criteria. Appendix a: seismic and geology siting criteria for nuclear power plants, US Nucl. Regul. Comm. NRC Regul. Guide 10CFR100, 1973.

Orozova, I. M. and Suhadolc, P.: A deterministic–probabilistic approach for seismic hazard assessment, Tectonophysics, 312, 191–202, https://doi.org/10.1016/S0040-1951(99)00162-6, 1999.

Ousadou, F., Dorbath, L., Ayadi, A., Dorbath, C., and Gharbi, S.: Stress field variations along the Maghreb region derived from inversion of major seismic crisis fault plane solutions, Tectonophysics, 632, 261–280, https://doi.org/10.1016/j.tecto.2014.06.017, 2014.

Pagani, M., Monelli, D., Weatherill, G., Danciu, L., Crowley, H., Silva, V., Henshaw, P., Butler, L., Nastasi, M., Panzeri, L., Simionato, M., and Vigano, D.: OpenQuake Engine: An Open Hazard (and Risk) Software for the Global Earthquake Model, Seismol. Res. Lett., 85, 692–702, https://doi.org/10.1785/0220130087, 2014.

Pagani, M., Garcia-Pelaez, J., Gee, R., Johnson, K., Poggi, V., Silva, V., Simionato, M., Styron, R., Viganò, D., Danciu, L., Monelli, D., and Weatherill, G.: The 2018 version of the Global Earthquake Model: Hazard component, Earthq. Spectra, 36, 226–251, https://doi.org/10.1177/8755293020931866, 2020.

Pailoplee, S., Sugiyama, Y., and Charusiri, P.: Deterministic and probabilistic seismic hazard analyses in Thailand and adjacent areas using active fault data, Earth Planets Space, 61, 1313–1325, https://doi.org/10.1186/BF03352984, 2009.

Palano, M., González, P. J., and Fernández, J.: Strain and stress fields along the Gibraltar Orogenic Arc: Constraints on active geodynamics, Gondwana Res., 23, 1071–1088, https://doi.org/10.1016/j.gr.2012.05.021, 2013.

Panza, G. F. and Bela, J.: NDSHA: A new paradigm for reliable seismic hazard assessment, Eng. Geol., 275, 105403, https://doi.org/10.1016/j.enggeo.2019.105403, 2020.

Panza, G. F., Prozorov, A. G., and Suhadolc, P.: Lithosphere structure and statistical properties of seismicity in Italy and surrounding regions, J. Geodyn., 12, 189–215, https://doi.org/10.1016/0264-3707(90)90007-H, 1990.

Panza, G. F., Vaccari, F., Costa, G., Suhadolc, P., and Fäh, D.: Seismic Input Modelling for Zoning and Microzoning, Earthq. Spectra, 12, 529–566, https://doi.org/10.1193/1.1585896, 1996.

Panza, G. F., Vaccari, F., and Cazzaro, R.: Deterministic Seismic Hazard Assessment, in: Vrancea Earthquakes: Tectonics, Hazard and Risk Mitigation: Contributions from the First International Workshop on Vrancea Earthquakes, Bucharest, Romania, November 1–4, 1997, edited by: Wenzel, F., Lungu, D., and Novak, O., Springer Netherlands, Dordrecht, 269–286, https://doi.org/10.1007/978-94-011-4748-4_25, 1999.

Panza, G. F., Romanelli, F., and Vaccari, F.: Seismic wave propagation in laterally heterogeneous anelastic media: Theory and applications to seismic zonation, in: Advances in Geophysics, vol. 43, edited by: Dmowska, R. and Saltzman, B., Elsevier, 1–95, https://doi.org/10.1016/S0065-2687(01)80002-9, 2001.

https://doi.org/10.5194/nhess-2023-52
Preprint. Discussion started: 4 April 2023


Natural Hazards and Earth System Sciences
Discussions

Panza, G. F., Mura, C. L., Peresan, A., Romanelli, F., and Vaccari, F.: Chapter Three - Seismic Hazard Scenarios as Preventive Tools for a Disaster Resilient Society, in: Advances in Geophysics, vol. 53, edited by: Dmowska, R., Elsevier, 93–165, https://doi.org/10.1016/B978-0-12-380938-4.00003-3, 2012.

Papadopoulos, G. A., Gràcia, E., Urgeles, R., Sallares, V., De Martini, P. M., Pantosti, D., González, M., Yalciner, A. C., Mascle, J., Sakellariou, D., Salamon, A., Tinti, S., Karastathis, V., Fokaefs, A., Camerlenghi, A., Novikova, T., and Papageorgiou, A.: Historical and pre-historical tsunamis in the Mediterranean and its connected seas: Geological signatures, generation mechanisms and coastal impacts, Mar. Geol., 354, 81–109, https://doi.org/10.1016/j.margeo.2014.04.014, 2014.

Pastor, A. R.: Traits sismiques de la Peninsule Iberique, Ateliers de l'Institut géographique et cadastral, 1927.

Poggi, V., Garcia-Peláez, J., Styron, R., Pagani, M., and Gee, R.: A probabilistic seismic hazard model for North Africa, Bull. Earthq. Eng., 18, 2917–2951, https://doi.org/10.1007/s10518-020-00820-4, 2020.

Ramkrishnan, R., Kolathayar, S., and Sitharam, T. G.: Probabilistic seismic hazard analysis of North and Central Himalayas using regional ground motion prediction equations, Bull. Eng. Geol. Environ., 80, 8137–8157, https://doi.org/10.1007/s10064-021-02434-9, 2021.

Reilly, W. I., Fredrich, G., Hein, G. W., Landau, H., Almazán, J. L., and Caturla, J. L.: Geodetic determination of crustal deformation across the Strait of Gibraltar, Geophys. J. Int., 111, 391–398, https://doi.org/10.1111/j.1365-246X.1992.tb00585.x, 1992.

Reiter, L.: Earthquake Hazard Analysis, Issues and Insights, Columbia U, Press N. Y. NY, 1990.

Rivas Medina, A.: Contribución metodológica para incorporar fallas activas en la modelización de la fuente dirigida a estimaciones de peligrosidad sísmica. Aplicación al sur de España, phd, E.T.S.I. en Topografía, Geodesia y Cartografía (UPM), 2014.

Rivas-Medina, A., Benito, B., and Gaspar-Escribano, J. M.: Approach for combining fault and area sources in seismic hazard assessment: application in south-eastern Spain, Nat. Hazards Earth Syst. Sci., 18, 2809–2823, https://doi.org/10.5194/nhess-18-2809-2018, 2018.

Rodriguez, M., Maleuvre, C., Jollivet-Castelot, M., d'Acremont, E., Rabaute, A., Lafosse, M., Ercilla, G., Vázquez, J.-T., Alonso, B., Ammar, A., and Gorini, C.: Tsunamigenic submarine landslides along the Xauen–Tofiño banks in the Alboran Sea (Western Mediterranean Sea), Geophys. J. Int., 209, 266–281, https://doi.org/10.1093/gji/ggx028, 2017.

Sá, L. F., Morales-Esteban, A., and Neyra, P. D.: A deterministic seismic risk macrozonation of Seville, Arab. J. Geosci., 14, 2392, https://doi.org/10.1007/s12517-021-08626-7, 2021.

Salgado Gálvez, M. A., Cardona Arboleda, O. D., Carreño Tibaduiza, M. L., and Barbat Barbat, H. A.: Probabilistic seismic hazard and risk assessment in Spain: national and local level case studies, Centre Internacional de Mètodes Numèrics en Enginyeria (CIMNE), 2015.

Silva, P. G., Elez, J., Giner-Robles, J., Perez-Lopez, R., Roquero, E., Rodriguez-Pascua, M., Azcárate, T., and Martínez-Graña, A.: ANÁLISIS GEOLÓGICO DEL TERREMOTO DE TORREVIEJA DE 1829 (ALICANTE, SE ESPAÑA), 2019.

Silva, V., Crowley, H., Varum, H., and Pinho, R.: Seismic risk assessment for mainland Portugal, Bull. Earthq. Eng., 13, 429–457, https://doi.org/10.1007/s10518-014-9630-0, 2015.

https://doi.org/10.5194/nhess-2023-52
Preprint. Discussion started: 4 April 2023

Sokolov, V. Y., Wenzel, F., and Mohindra, R.: Probabilistic seismic hazard assessment for Romania and sensitivity analysis: A case of joint consideration of intermediate-depth (Vrancea) and shallow (crustal) seismicity, Soil Dyn. Earthq. Eng., 29, 364–381, https://doi.org/10.1016/j.soildyn.2008.04.004, 2009.

Somoza, L., Medialdea, T., Terrinha, P., Ramos, A., and Vázquez, J.-T.: Submarine Active Faults and Morpho-Tectonics Around the Iberian Margins: Seismic and Tsunamis Hazards, Front. Earth Sci., 9, 2021.

Soumaya, A., Ben Ayed, N., Rajabi, M., Meghraoui, M., Delvaux, D., Kadri, A., Ziegler, M., Maouche, S., and Braham, A.: Active Faulting Geometry and Stress Pattern Near Complex Strike-Slip Systems Along the Maghreb Region: Constraints on Active Convergence in the Western Mediterranean, Tectonics, 37, 3148–3173, https://doi.org/10.1029/2018TC004983, 2018.

Stein, S., Geller, R. J., and Liu, M.: Why earthquake hazard maps often fail and what to do about it, Tectonophysics, 562–563, 1–25, https://doi.org/10.1016/j.tecto.2012.06.047, 2012.

Stich, D., Batlló, J., Morales, J., Macià, R., and Dineva, S.: Source parameters of the MW= 6.1 1910 Adra earthquake (southern Spain), Geophys. J. Int., 155, 539–546, https://doi.org/10.1046/j.1365-246X.2003.02059.x, 2003.

Stich, D., Serpelloni, E., de Lis Mancilla, F., and Morales, J.: Kinematics of the Iberia–Maghreb plate contact from seismic moment tensors and GPS observations, Tectonophysics, 426, 295–317, https://doi.org/10.1016/j.tecto.2006.08.004, 2006.

Suhadolc, P.: Fault-plane solutions and seismicity around the EGT southern segment, R Freeman St Mueller Ed. Proc. Sixth Workshop Eur. Geotraverse Proj. Eur. Sci. Found. Strasbg., 371–382, 1990.

Süli, E. and Mayers, D. F.: An Introduction to Numerical Analysis, Cambridge University Press, 440 pp., 2003.

Tehseen, R., Farooq, M. S., and Abid, A.: Earthquake Prediction Using Expert Systems: A Systematic Mapping Study, Sustainability, 12, 2420, https://doi.org/10.3390/su12062420, 2020.

Toro, G. R., Abrahamson, N. A., and Schneider, J. F.: Model of Strong Ground Motions from Earthquakes in Central and Eastern North America: Best Estimates and Uncertainties, Seismol. Res. Lett., 68, 41–57, https://doi.org/10.1785/gssrl.68.1.41, 1997.

Tozer, B., Sandwell, D. T., Smith, W. H. F., Olson, C., Beale, J. R., and Wessel, P.: Global Bathymetry and Topography at 15 Arc Sec: SRTM15+, Earth Space Sci., 6, 1847–1864, https://doi.org/10.1029/2019EA000658, 2019.

US NRC: Identification and characterization of seismic sources and determination of safe shutdown earthquake ground motion, US Nucl. Regul. Comm. NRC Regul. Guide 1165, 1997.

USCOLD: Committee on Earthquakes. Guidelines for earthquake design and evaluation of structures appurtenant to dams, US Comm. Large Dams USCOLDDenver CO, 75 pp., 1995.

Vázquez, J. T. and Vegas Martínez, R.: Acomodación de la convergencia entre África y la Península Ibérica, Golfo de Cádiz y Mar de Alborán, a partir del análisis de terremotos., Geogaceta, 172–174, 1999.

Vázquez, J. T. (Juan T., Galindo-Zaldívar, J., Palomino, D. (Desirée), González, L., Fernández-Puga, M. C., Naranjo, S., Pedrosa, M. T., Tendero-Salmerón, V., Bárcenas-Gascón, P. (Patricia), Estrada, F., and Ercilla, G.: SISTEMA DE PLIEGUES ACTIVOS EN EL MARGEN CONTINENTAL SEPTENTRIONAL DEL MAR DE ALBORÁN (MEDITERRANEO OCCIDENTAL), Servicio de Publicaciones de la Universidad de Zaragoza, 2022a.

Vázquez, J.-T., Ercilla, G., Alonso, B., Peláez, J. A., Palomino, D., León, R., Bárcenas, P., Casas, D., Estrada, F., Fernández-Puga, M. C., Galindo-Zaldívar, J., Henares, J., Llorente, M., Sánchez-Guillamón, O., d'Acremont, E., Ammar, A., Chourak, M., Fernández-Salas, L. M., López-González, N., and Lafuerza, S.: Triggering Mechanisms of Tsunamis in the Gulf of Cadiz and the Alboran Sea: An Overview, in: Historical Earthquakes, Tsunamis and Archaeology in the Iberian Peninsula, edited by: Álvarez-Martí-Aguilar, M. and Machuca Prieto, F., Springer Nature, Singapore, 65–104, https://doi.org/10.1007/978-981-19-1979-4_4, 2022b.

Vilanova, S. P.: The Seismicity of the Iberian Peninsula and interpretation of its genesis: implications for seismic hazard assessment, in: IX Simpósio sobre a Margem Ibérica Atlântica IX Simposio sobre el Margen Ibérico Atlántico IX Symposium on the Iberian Atlantic Margin, 25, 2018.

Vilanova, S. P. and Fonseca, J. F. B. D.: Probabilistic Seismic-Hazard Assessment for Portugal, Bull. Seismol. Soc. Am., 97, 1702–1717, https://doi.org/10.1785/0120050198, 2007.

Vilanova, S. P. and Fonseca, J. F. B. D.: Ground-Motion Models for Seismic-Hazard Assessment in Western Iberia: Constraints from Instrumental Data and Intensity Observations, Bull. Seismol. Soc. Am., 102, 169–184, https://doi.org/10.1785/0120110097, 2012.

Villaverde, R.: Fundamental Concepts of Earthquake Engineering, CRC Press, 976 pp., 2009.

Vipin, K. S.: Assessment Of Seismic Hazard With Local Site Effects : Deterministic And Probabilistic Approaches, Thesis, 2013.

Wang, J. P. and Huang, D.: Deterministic seismic hazard assessments for Taiwan considering non-controlling seismic sources, Bull. Eng. Geol. Environ., 73, 635–641, https://doi.org/10.1007/s10064-013-0491-6, 2014.

Wang, J.-P., Huang, D., and Yang, Z.: Deterministic seismic hazard map for Taiwan developed using an in-house Excel-based program, Comput. Geosci., 48, 111–116, https://doi.org/10.1016/j.cageo.2012.05.014, 2012.

Wang, Y., Wang, R., and Zhang, J.-M.: Large-scale seismic seafloor stability analysis in the South China Sea, Ocean Eng., 235, 109334, https://doi.org/10.1016/j.oceaneng.2021.109334, 2021.

Wang, Z.: Comment on "PSHA Validated by Quasi Observational Means" by R. M. W. Musson, Seismol. Res. Lett., 83, 714–716, https://doi.org/10.1785/0220120016, 2012.

Wang, Z. and Cobb, J. C.: A critique of probabilistic versus deterministic seismic hazard analysis with special reference to the New Madrid seismic zone, Recent Adv. North Am. Paleoseismology Neotectonics East Rock., 2012.

Woessner, J., Laurentiu, D., Giardini, D., Crowley, H., Cotton, F., Grünthal, G., Valensise, G., Arvidsson, R., Basili, R., Demircioglu, M. B., Hiemer, S., Meletti, C., Musson, R. W., Rovida, A. N., Sesetyan, K., Stucchi, M., and The SHARE Consortium: The 2013 European Seismic Hazard Model: key components and results, Bull. Earthq. Eng., 13, 3553–3596, https://doi.org/10.1007/s10518-015-9795-1, 2015.

Worden, C. B., Thompson, E. M., Hearne, M., and Wald, D. J.: ShakeMap Manual Online: technical manual, user's guide, and software guide, US Geological Survey, 2020.

Youngs, R. R., Chiou, S.-J., Silva, W. J., and Humphrey, J. R.: Strong Ground Motion Attenuation Relationships for Subduction Zone Earthquakes, Seismol. Res. Lett., 68, 58–73, https://doi.org/10.1785/gssrl.68.1.58, 1997.

https://doi.org/10.5194/nhess-2023-52
Preprint. Discussion started: 4 April 2023

Zengaffinen-Morris, T., Urgeles, R., and Løvholt, F.: On the Inference of Tsunami Uncertainties From Landslide Run-Out Observations, J. Geophys. Res. Oceans, 127, e2021JC018033, https://doi.org/10.1029/2021JC018033, 2022.

Zhao, J. X., Zhang, J., Asano, A., Ohno, Y., Oouchi, T., Takahashi, T., Ogawa, H., Irikura, K., Thio, H. K., Somerville, P. G., Fukushima, Y., and Fukushima, Y.: Attenuation Relations of Strong Ground Motion in Japan Using Site Classification Based on Predominant Period, Bull. Seismol. Soc. Am., 96, 898–913, https://doi.org/10.1785/0120050122, 2006.

Zulkifli, M., Rudyanto, A., and Sakti, A.: The view of seismic hazard in the Halmahera region, 050004 pp., https://doi.org/10.1063/1.4987082, 2017.